AGU PUBLICATIONS

Global Biogeochemical Cycles

RESEARCH ARTICLE
10.1002/2015GB005357

**Key Points:**
- Elevated dFe in the Chilean ODZ is derived from porewater but is redox cycled on short spatiotemporal scales
- Vanishingly low dFe in the surface gyre is dominated by horizontal fluxes and less by dust inputs
- Hydrothermal-derived deep dFe is isotopically heavy in the South Pacific, while it has near-crustal isotope composition at Station ALOHA

**Supporting Information:**
- Supporting Information S1
- Data Set S1

**Correspondence to:**
J. N. Fitzsimmons,
jessfitz@tamu.edu

**Citation:**
Fitzsimmons, J. N., T. M. Conway, J.-M. Lee, R. Kayser, K. M. Thyng, S. G. John, and E. A. Boyle (2016), Dissolved iron and iron isotopes in the southeastern Pacific Ocean, *Global Biogeochem. Cycles*, *30*, 1372–1395, doi:10.1002/2015GB005357.

Received 18 DEC 2015
Accepted 11 SEP 2016
Accepted article online 14 SEP 2016
Published online 5 OCT 2016



# Dissolved iron and iron isotopes in the southeastern Pacific Ocean

**Jessica N. Fitzsimmons[1,2], Tim M. Conway[3,4,5], Jong-Mi Lee[2,6], Richard Kayser[2], Kristen M. Thyng[1], Seth G. John[3,7], and Edward A. Boyle[2]**

[1]Now at Department of Oceanography, Texas A&M University, College Station, Texas, USA, [2]Department of Earth, Atmospheric, and Planetary Sciences, Massachusetts Institute of Technology, Cambridge, Massachusetts, USA, [3]Department of Earth and Ocean Sciences, University of South Carolina, Columbia, South Carolina, USA, [4]Department of Earth Sciences, ETH Zürich, Zurich, Switzerland, [5]Now at College of Marine Science, University of South Florida, St. Petersburg, Florida, USA, [6]Now at Department of Ocean Sciences, University of California, Santa Cruz, California, USA, [7]Now at Department of Earth Sciences, University of Southern California, Los Angeles, California, USA

**Abstract** The Southeast Pacific Ocean is a severely understudied yet dynamic region for trace metals such as iron, since it experiences steep redox and productivity gradients in upper waters and strong hydrothermal iron inputs to deep waters. In this study, we report the dissolved iron (dFe) distribution from seven stations and Fe isotope ratios ($\delta^{56}$Fe) from three of these stations across a near-zonal transect from 20 to 27°S. We found elevated dFe concentrations associated with the oxygen-deficient zone (ODZ), with light $\delta^{56}$Fe implicating porewater fluxes of reduced Fe. However, temporal dFe variability and rapid $\delta^{56}$Fe shifts with depth suggest gradients in ODZ Fe source and/or redox processes vary over short-depth/spatial scales. The dFe concentrations decreased rapidly offshore, and in the upper ocean dFe was controlled by biological processes, resulting in an Fe:C ratio of 4.2 μmol/mol. Calculated vertical diffusive Fe fluxes were greater than published dust inputs to surface waters, but both were orders of magnitude lower than horizontal diffusive fluxes, which dominate dFe delivery to the gyre. The $\delta^{56}$Fe data in the deep sea showed evidence for a −0.2‰ Antarctic Intermediate Water end-member and a heavy $\delta^{56}$Fe of +0.55‰ for distally transported hydrothermal dissolved Fe from the East Pacific Rise. These heavy $\delta^{56}$Fe values were contrasted with the near-crustal $\delta^{56}$Fe recorded in the hydrothermal plume reaching Station ALOHA in the North Pacific. The heavy hydrothermal $\delta^{56}$Fe precludes a nanopyrite composition of hydrothermal dFe and instead suggests the presence of oxides or, more likely, binding of hydrothermal dFe by organic ligands in the distal plume.

## 1. Introduction

The subtropical Southeast Pacific Ocean is one of the most understudied regions of the global ocean, yet it encompasses enormous biogeochemical diversity [*Claustre et al.*, 2008]. Two opposing biogeochemical regimes share this region: the Southeast Pacific subtropical gyre in the central South Pacific and the permanent upwelling and oxygen minimum zone along the South American coast. The South Pacific subtropical gyre is the largest of the world's gyres and also the most oligotrophic, with the lowest marine chlorophyll *a* concentrations yet reported (0.019 mg chlorophyll *a* $m^{-3}$) found near Eastern Island [*Claustre et al.*, 2008]. In contrast, the wind-driven upwelling along the Chilean coast fuels some of the highest rates of primary production in the ocean [*Carr*, 2001]. This organic material sinks and is remineralized at high rates, depleting the oxygen inventory, which combined with poor ventilation produces an oxygen-deficient zone (ODZ) that reaches nearly complete anoxia [*Fuenzalida et al.*, 2009]. Thus, across the Southeast Pacific chlorophyll *a* concentrations range over 2 orders of magnitude, and the redox gradient spans from complete to vanishing oxygenation, providing an impressive biogeochemical gradient for study.

The Southeast Pacific is also one of the most understudied regions globally for trace metals, with few reported dissolved iron (dFe) measurements below 500 m depth (see existing global data compilations in, e.g., *Moore and Braucher* [2008] and *Tagliabue et al.* [2012]). Thus, despite recent efforts to explore Fe cycling through the international GEOTRACES program [*Mawji et al.*, 2015] and to integrate it into global biogeochemical models, we still lack a detailed understanding of the processes controlling the Fe distribution in this region. It is now well established that low Fe concentrations can limit primary production and nitrogen fixation in high-nutrient, low-chlorophyll regions due to the requirement for Fe in the photosynthetic apparatus and the nitrogenase enzyme required for nitrogen fixation [*Martin and Fitzwater*, 1988; *Sunda*, 2012]. In

the remote waters of the oligotrophic South Pacific subtropical gyre, Fe fluxes are low: aerosol deposition in the South Pacific is among the lowest in the world [*Wagener et al.*, 2008], and offshore Fe gradients from the South American continent have been shown to be steep [*Bruland et al.*, 2005], potentially limiting the potential for significant transport of continental and/or ODZ Fe offshore to the gyre. One study documented very low concentrations of dFe in the upper 400 m of the gyre (0.05–0.10 nmol/kg [*Blain et al.*, 2008]), yet surprisingly incubation studies from the same cruise observed limited response to Fe enrichment by surface phytoplankton in 7 day incubations along the edges of the gyre [*Bonnet et al.*, 2008]. Instead, short-term primary production in the heart of the gyre was controlled by nitrate availability.

Nonetheless, even if Fe is not the nutrient most limiting phytoplankton productivity, in general its concentrations in the South Pacific gyre are extremely low and are certainly involved in the generation of nitrate through the Fe-intensive nitrogen fixation process; thus, Fe is essential for gyre microorganisms. In fact, models of nutrient limitation project Fe to be the limiting nutrient for diazotrophs across this entire region [*Moore et al.*, 2002]. So how is Fe supplied to microorganisms of South Pacific gyre surface waters? The most directly bioavailable form of Fe, Fe(II) [*Morel et al.*, 2008], is stable only in waters with very low oxygen concentrations, such as those of the Peruvian ODZ, and thus, the continental margin and ODZ waters are a large potential source of Fe to the South Pacific gyre. Accordingly, most of the published studies of Fe in the Southeast Pacific region have focused on the redox dynamics of the Eastern Tropical Pacific ODZ [*Bruland et al.*, 2005; *Hong and Kester*, 1986; *Vedamati et al.*, 2014] and have recorded highly elevated dFe concentrations (2–150 nM) rich in Fe(II). Following this, the relationships between Fe redox chemistry and offshore transport across the redox gradients are of great interest for constraining the Fe cycle in this region and understanding the potential for these margin Fe sources to supply Fe to the gyre. A further recently identified source of dFe in this region is the transport of hydrothermal Fe from the nearby East Pacific Rise, which contributes significantly to Fe concentrations at 2000–2500 m depth [*Fitzsimmons et al.*, 2014; *Resing et al.*, 2015]. While the effect of this abyssal dFe source on the Fe budget in surface waters is to date only estimated by models [*Saito et al.*, 2013; *Tagliabue et al.*, 2010], it has recently been hypothesized in the "leaky vent hypothesis" that hydrothermal dFe may contribute significantly to the global dFe inventory [*Toner et al.*, 2012]. Following this, it has become a research priority to investigate the chemical processes that stabilize hydrothermal Fe, how it may be transformed or removed during transport, and how it may contribute to primary production in surface waters upon upwelling.

In this paper, we present dissolved Fe concentration profiles across the upper 1000 m for seven stations, extending to full depth for three of these stations, along a transect from offshore South America into the South Pacific gyre (Figure 1). Two of these full-depth profiles were recently used to demonstrate the transport of hydrothermally sourced Fe from the East Pacific Rise to this region [*Fitzsimmons et al.*, 2014]. Here we extend that data set to provide a more comprehensive view of the sources and cycling of Fe in this poorly understood region of the Pacific, especially in the understudied surface waters of the Southeast Pacific subtropical gyre. We compare our results both spatially and temporally with those of the existing dFe data from the literature in order to assess the significance of various Fe sources to the gyre. We also present new dissolved stable Fe isotope ratio data ($\delta^{56}$Fe relative to IRRM-014) from the three full-depth profiles. Seawater-dissolved $\delta^{56}$Fe data have been used previously as an Fe source "fingerprinting" tool within the water column, providing new insight into the marine cycling of Fe in the open ocean [*Chever et al.*, 2015; *Conway and John*, 2014; *John and Adkins*, 2012; *Labatut et al.*, 2014; *Mawji et al.*, 2015; *Radic et al.*, 2011]. Seawater-dissolved $\delta^{56}$Fe measurements are particularly useful for tracing dissolved Fe from reducing sediment porewaters, which have been characterized with a $\delta^{56}$Fe signature as light as −4‰ [*Homoky et al.*, 2009; *Severmann et al.*, 2006] and also have been invoked to explain the light-dissolved $\delta^{56}$Fe in low-oxygen waters along both the North and South American margins (−0.3 to −1.8‰ [*Chever et al.*, 2015; *John et al.*, 2012]). Here we use $\delta^{56}$Fe and dFe flux estimates to assign and quantitatively compare the sources of dFe to the Southeast Pacific Ocean in order to provide a more synthetic view of Fe cycling within this region.

## 2. Methods

### 2.1. Sampling Methods

Seawater samples from the Southeast Pacific Ocean were collected on the BiG RAPA cruise (Biogeochemical Gradients: Role in Arranging Planktonic Assemblages), organized by the Center for Microbial Oceanography: Research and Educate (C-MORE), on 18 November to 13 December 2010 (Chief Scientist: D. Repeta). The

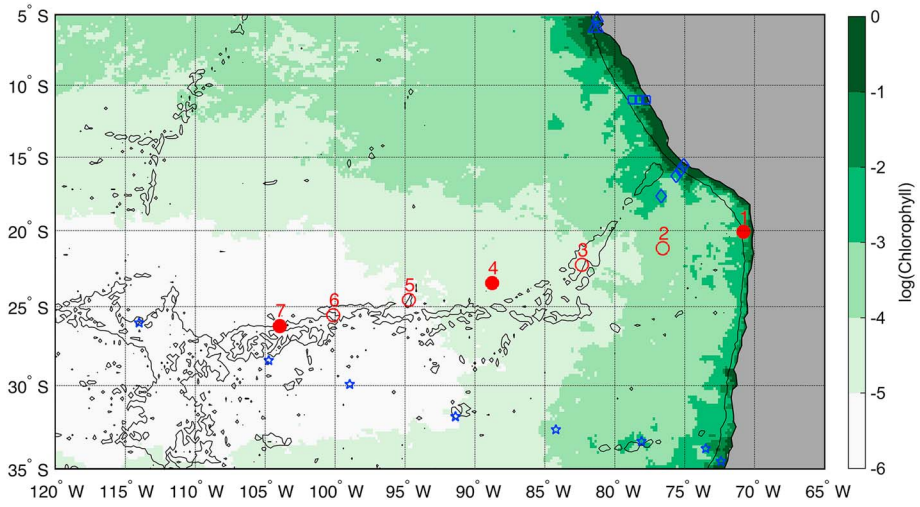


**Figure 1.** Locations of stations sampled for trace metals in the subtropical Southeast Pacific overlain on the November 2010 Aqua Moderate Resolution Imaging Spectroradiometer satellite-derived chlorophyll concentrations map, which is plotted in green on a log scale. The red dots show the stations sampled in this BiG RAPA study, where the filled dots represent stations that were sampled to the bottom and the open dots represent stations that were sampled to 1000 m. The station locations of past cruises to this region, which are referenced in this paper, are plotted as smaller open blue symbols: BIOSOPE stations of *Blain et al.* [2008] are shown as stars, KN182-09 stations of *Vedamati et al.* [2014] in the Peruvian ODZ are shown as diamonds, Peruvian ODZ stations of *Chever et al.* [2015] are shown as triangles, and sediment core stations of *Scholz et al.*, 2011 are shown as squares. The 3000 m bathymetric contour is indicated by a black line, which highlights the hydrothermally active, meridional East Pacific Rise near 115°W and the (to date presumed) non-hydrothermal Sala y Gomez and Nazca Ridges near 25°S.

cruise track proceeded from east to west and included seven stations (Figure 1), three of which were sampled to the bottom (Stations 1, 4, and 7) and the remainder only to 1000 m depth. Trace metal clean samples were collected using two sampling systems that have been described previously: the MITESS Vane system [*Bell et al.*, 2002; *Fitzsimmons et al.*, 2013] and a rosette of 12 Niskin-X bottles mounted on an epoxy-coated frame and deployed on a Kevlar hydrowire [*Noble et al.*, 2012]. These systems have been shown to produce equivalent uncontaminated seawater samples in the past [*Fitzsimmons and Boyle*, 2012], and they will be treated interchangeably for the remainder of this paper.

Upon recovery, Niskin or MITESS bottles were carried into a high-efficiency particulate arrestance-filtered (HEPA) sampling space constructed aboard the ship, and seawater was immediately filtered through 0.4 μm Nuclepore® membrane (to define the dissolved Fe (dFe) fraction) and 0.02 μm Anodisc (to define the soluble Fe (sFe) fraction) filters. Filtration was completed within 1 h of recovery for low-oxygen samples, which has been shown to reduce sampling artifacts on prior cruises [*Sedwick et al.*, 2015]. High-density polyethylene subsample bottles had been precleaned in 10% vol/vol reagent grade hydrochloric acid (HCl) at 60°C overnight, rinsed in ultrapure water, and then recleaned in 0.01% vol/vol ultrapure HCl at 60°C overnight before use. Each bottle was rinsed with sample seawater prior to filling, and within a few days of collection samples were acidified to pH 2 by using ultrapure HCl. Ultrapure 6 M HCl was obtained by four consecutive distillations of reagent grade HCl in a Vycor® still. This HCl was verified to have low-Fe blanks (adding ~0.0001 nmol/kg to a seawater sample, $<$1% of the lowest sample Fe concentration reported here) by inductively coupled plasma mass spectrometry (ICP–MS) analysis after evaporation to dryness and re-dissolution in 0.1 M $HNO_3$, achieving a tenfold preconcentration. Fe isotope samples were also collected at Station ALOHA (22.75°N, 158°W) north of the Hawaiian Island of Oahu on 22 July 2012 as a part of the Center for Microbial Oceanography: Research and Education (C-MORE) HOE-DYLAN VII cruise [*Fitzsimmons et al.*, 2015b] using the MITESS Vanes system as described above.

### 2.2. Analytical Methods

Fe concentration analyses were made using the isotope dilution ICP–MS method of *Lee et al.* [2011]. This method employs a $^{54}$Fe isotope spike and batch Fe preconcentration onto nitrilotriacetate resin beads,

followed by analysis on a hexapole collision cell IsoProbe multiple-collector ICP–MS (MC–ICP–MS) instrument, using Ar and $H_2$ gas in the hexapole to minimize the $^{40}Ar^{16}O^+$ interference on $^{56}Fe^+$. The dFe concentration profiles for Stations 4 and 7 are reproduced from *Fitzsimmons et al.* [2014] and were measured alongside the other dFe data presented here. Replicate analyses of the SAFe D2 standard reference material during the relevant analytical sessions, 0.925 ± 0.041 nmol/kg ($n = 23$), are in good agreement with the most recent consensus value of 0.933 ± 0.023 nmol/kg (May 2013; www.geotraces.org/science/intercalibration). Replicate analyses of SAFe surface seawater averaging 0.087 ± 0.049 nmol/kg ($n = 48$) are also in good agreement with the recent SAFe S consensus value of 0.093 ± 0.008 nmol/kg.

Dissolved Fe stable isotope ratio analyses were conducted on 0.4 μm filtered dissolved seawater samples in the Marine Trace Element Laboratory and Center for Elemental Mass Spectrometry laboratory at the University of South Carolina following the methods described in *Conway et al.* [2013]. This method involves addition of a $^{57}Fe$-$^{58}Fe$ double spike in a 1:2 sample:spike concentration ratio, batch preconcentration onto Nobias PA-1 chelating resin, and purification for Fe by anion-exchange chromatography with AGMP-1 resin. Purified samples were analyzed by using a Thermo Neptune MC–ICP–MS in high-resolution mode, with a jet interface and Apex-Q (Elemental Scientific, Omaha, NE) desolvation system without membrane. Isobaric interferences from Ni and Cr were corrected by monitoring $^{60}Ni$ and $^{53}Cr$. Stable Fe isotope ratios were calculated by using a data reduction scheme following the iterative method of *Siebert et al.* [2001] and are reported as $\delta^{56}Fe$ in standard delta notation (‰) relative to the IRMM-014 isotope standard:

$$\delta^{56}Fe\left(^{0}/_{00}\right) = \left[\frac{\frac{^{56}Fe}{^{54}Fe}_{sample}}{\frac{^{56}Fe}{^{54}Fe}_{IRMM-014}} - 1\right] * 1000$$

We express uncertainty on $\delta^{56}Fe$ in figures and in the supporting information in this study with the $2\sigma$ standard internal error calculated from samples and bracketing standards [*Conway et al.*, 2013], based on the previous observation that internal error dominates uncertainty with this technique [*John*, 2012]. The $2\sigma$ internal errors in this study varied from 0.03 to 0.18‰, dependent largely on Fe concentration (see supporting information). As an indication of external precision for these samples we calculated the 2 SD of the offset of duplicate analyses from the mean of each sample in this study (>0.1 nmol/kg) following *Steele et al.* [2011], excluding two low concentration samples which have accordingly larger internal errors. This value for external precision (0.07‰), which was calculated from duplicate ICP–MS analyses of 42 samples over four analytical sessions, with most duplicates analyzed in different sessions, is similar in size to internal error for most samples but should be considered as a more conservative estimate of uncertainty when larger than internal error. Both internal errors and this measure of external precision are much smaller than the variability observed in $\delta^{56}Fe$ in the water column profiles in this study (−0.8 to +0.5‰), demonstrating the suitability of this method to investigate variability in $\delta^{56}Fe$ in the oceans.

### 2.3. Modified Optimum Multi-Parameter Analysis of Water Type

Following *Jenkins et al.* [2015], we identified the relative influence of various water masses along the BiG RAPA section by applying a modified version of the Optimum Multi-Parameter Analysis (mOMPA) that has been in use for decades [*Mackas et al.*, 1987; *Tomczak*, 1981]. This method determines a least squares solution to the fraction of various water masses, defined quantitatively by using an assigned end-member composition, for any given depth and location along a section of observed, conservative hydrographic properties. This method must utilize at least the number of hydrographic properties as there are water masses in a given region in order to overdetermine the OMPA solution. Thus, we use four properties that are assumed to behave conservatively along our section: potential temperature ($\theta$), salinity ($S$), $P^*$, and SiO, where $P^*$ is equal to [*Broecker et al.*, 1991]

$$P^* = [\text{phosphate}] + [\text{dissolved oxygen}]/170 - 1.95$$

where 170 is an updated Redfield $O_2$/P ratio [*Anderson and Sarmiento*, 1994], and where SiO is defined as [*Broecker*, 1974]

$$SiO = [O_2] + [Si]*15$$

where 15 is equal to 150/10, a Redfield O2/Si ratio. These macronutrient terms are assumed to be have

**Table 1.** OMPA Water Mass End-Member Compositions

| Water Mass | $\theta$ (°C) | S | $O_2$ (μmol/kg) | Phosphate (μmol/kg) | Silicate (μmol/kg) | Ref | P* | SiO |
|---|---|---|---|---|---|---|---|---|
| STSW | 22 | 36.0 | 220 | 0.2 | 0.5 | a,b,c | −0.456 | 228 |
| SAAW | 11.5 | 33.8 | 268 | 1.07 | 2.17 | b,c | 0.696 | 301 |
| ESSW | 12 | 34.9 | 1 | 2.43 | 29.8 | b,c | 0.486 | 448 |
| AAIW | 5.5 | 34.2 | 238 | 1.97 | 24.6 | a,b,c | 1.420 | 607 |
| PDW | 1.8 | 34.7 | 105 | 2.76 | 157.3 | a,b,c | 1.428 | 2465 |
| Weight | 100 | 100 | | | | | 10 | 10 |

[a] *Fiedler and Talley* [2006].
[b] *Silva et al.* [2009].
[c] *Llanillo et al.* [2013].

conservatively because any biological uptake or remineralization would affect both the oxygen and P or Si terms equally. This results in the following OMPA constraint equations:

$$f_1\theta_1 + f_2\theta_2 + f_3\theta_3 + f_4\theta_4 = \theta + \varepsilon\theta$$
$$f_1S_1 + f_2S_2 + f_3S_3 + f_4S_4 = S + \varepsilon_S$$
$$f_1P*_1 + f_2P*_2 + f_3P*_3 + f_4P*_4 = P* + \varepsilon_{P*}$$
$$f_1\mathrm{SiO}_1 + f_2\mathrm{SiO}_2 + f_3\mathrm{SiO}_3 + f_4\mathrm{SiO}_4 = \mathrm{SiO} + \varepsilon_{\mathrm{SiO}}$$
$$f_1 + f_2 + f_3 + f_4 = 1 + \varepsilon_f$$
$$f_i > 0$$

where $f_i$ is the fractional contribution of each *i*th water mass. The $\varepsilon$ term in each equation is the residual error in the property balance that comprises both measurement error and uncertainty in the assignment of water mass end-member properties and/or unassigned water masses.

The OMPA model is a modified (mOMPA) because of the additional constraint of potential density anomaly ($\sigma_\theta$ relative to the surface) in order to overconstrain the model. The BiG RAPA section was broken into two vertical domains: an upper domain with $\sigma_\theta < 26.4$, which included contributions from Subtropical Surface Water (STSW), Equatorial Subsurface Water (ESSW), and Subantarctic Water (SAAW), and a lower domain with $\sigma_\theta > 26.4$, which included contributions from ESSW, SAAW, Antarctic Intermediate Water (AAIW), and Pacific Deep Water (PDW). The end-member compositions of these water masses are shown in Table 1, along with the literature references from which they were assigned. The weights indicated for each water mass property were assigned after consideration of respective analytical and sampling errors, the degree of uncertainty in the property assignments for each water mass, and the extent to which that property is conserved in the ocean. The property balance was assigned a weight equal to that of the highest weighted property.

## 3. Results and Discussion

The primary goal of this study was to expand our understanding of the distribution, sources, and sinks of dissolved Fe across the extreme oxygen and productivity gradients in the subtropical southeastern Pacific. We first describe the circulation of this region, followed by a description of Fe sources and cycling in the nearshore oxygen minimum zone. We then describe Fe sources to offshore waters of the gyre, with an emphasis on how oxygen and diffusive fluxes control these distributions. Finally, we finish with an assessment of how the deep ocean-dissolved $\delta^{56}$Fe measurements reported here inform our understanding of Fe cycling in the previously documented abyssal hydrothermal plume that extends eastward from the East Pacific Rise south of 20°S into this region [*Fitzsimmons et al.*, 2014], with comparison to new dissolved $\delta^{56}$Fe data from the Loihi Seamount hydrothermal plume near Hawaii in the North Pacific.

### 3.1. mOMPA Results and Regional Circulation

Several water masses comprise the upper 1000 m waters of the Southeast Pacific Ocean, which are summarized quantitatively over the BiG RAPA cruise transect in the OMPA model results shown in Figure 2, which were analyzed by using the hydrographic data in Figure 3 (along with a map indicating the general direction that each water mass flows). The upper ocean water masses are circulated by the Humboldt Current System, which is the northernmost of two circulatory branches that arise when the Antarctic Circumpolar Current

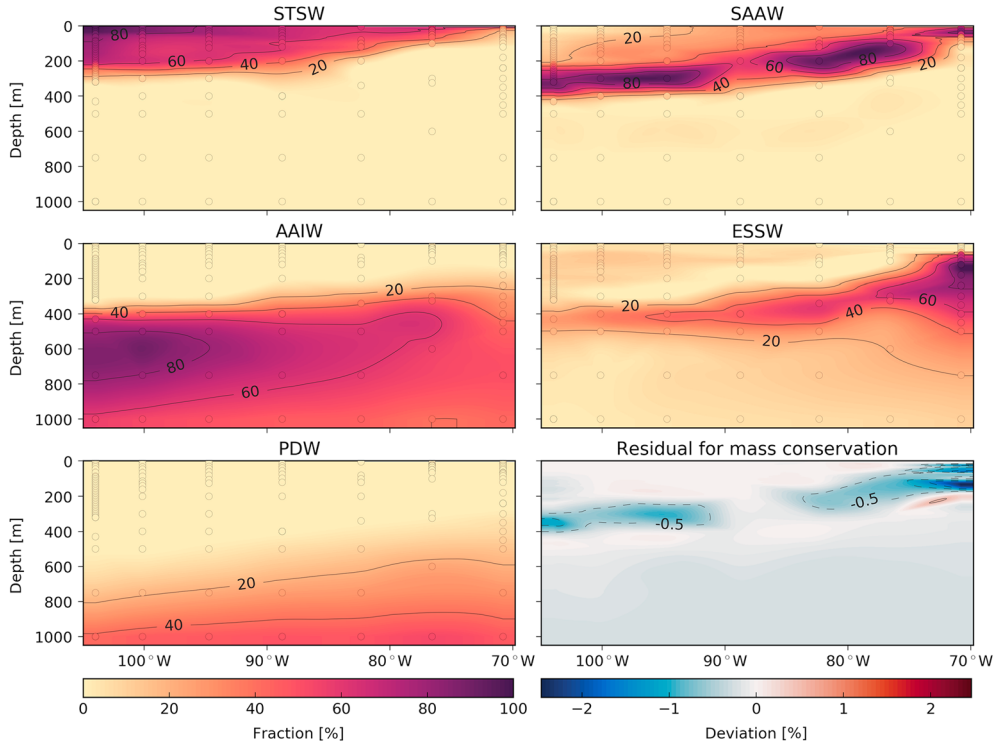


**Figure 2.** Modified Optimum Multi-Parameter Assessment (mOMPA) results showing the fraction of each water mass that is present at each of the sampling depths on the BiG RAPA cruise transect. The residual error in mass conservation is also plotted in percent and is very low. Water masses include Subtropical Surface Water (STSW), Equatorial Subsurface Water (ESSW), Subantarctic Water (SAAW), Antarctic Intermediate Water (AAIW), and Pacific Deep Water (PDW). The flow direction of each of these water masses is shown in Figure 3, along with the hydrographic data used to generate the OMPA model.

meets the South American continent near 45°S [*Silva et al.*, 2009]. The surface water of the subtropical gyre is composed of warm, saline Subtropical Surface Water (STSW), which forms along the northern edge of the South Pacific gyre in areas of high irradiation and evaporation [*Fiedler and Talley*, 2006]; STSW is then transported poleward across the South Pacific gyre and also along the South American Continent with the Peru Countercurrent [*Silva et al.*, 2009]. The ODZ, in contrast, is composed of Equatorial Subsurface Water (ESSW), which is a high-salinity, low-oxygen water mass that is advected poleward with the Peru-Chile Undercurrent. In between these water masses is the low-salinity Subantarctic Water (SAAW), which forms in the subtropical convergence ~35°S and flows northward with the Humboldt Current along the 26.2 isopycnal. Below, Antarctic Intermediate Water (AAIW), present from ~400 to 1000 m, is a low-salinity, high-oxygen water mass formed near the subtropical convergence of the SE Pacific that generally flows to the northeast. The ODZ is ventilated by AAIW from below and SAAW from above. Finally, below ~1000 m depth, AAIW transitions into Pacific Deep Water (PDW). The abyssal circulation at the deep stations of this study generally flows southeastward from 1000 to ~3000 m depth [*Reid*, 1997], streaming hydrothermally influenced waters from the East Pacific Rise into the Peru/Chile Basin south of 20°S [*Fitzsimmons et al.*, 2014].

### 3.2. The ODZ: Station 1

The Southeast Pacific Ocean ODZ close to South America (Figure 3) forms when equatorward winds promote offshore Ekman transport within the Peru Coastal Current. This process drives upwelling of nutrient-replete, thermocline waters to the surface (visible as a shoaled nutricline: Station 1, Figure 3), which results in rich phytoplankton productivity in these coastal waters. Remineralization of this sinking biological debris leads to severe oxygen consumption below, which combined with the poor ventilation of these waters produces the water column ODZ [*Karstensen et al.*, 2008]. In addition, continental shelf sediments along the Chilean/Peruvian coasts reach anoxic conditions [*Scholz et al.*, 2014] through the same supply of organic material and remineralization in sediment porewaters, using all available oxygen and quickly requiring microbes to turn to dissimilatory Mn and Fe redox cycling for energy. The resultant products of these biological processes,

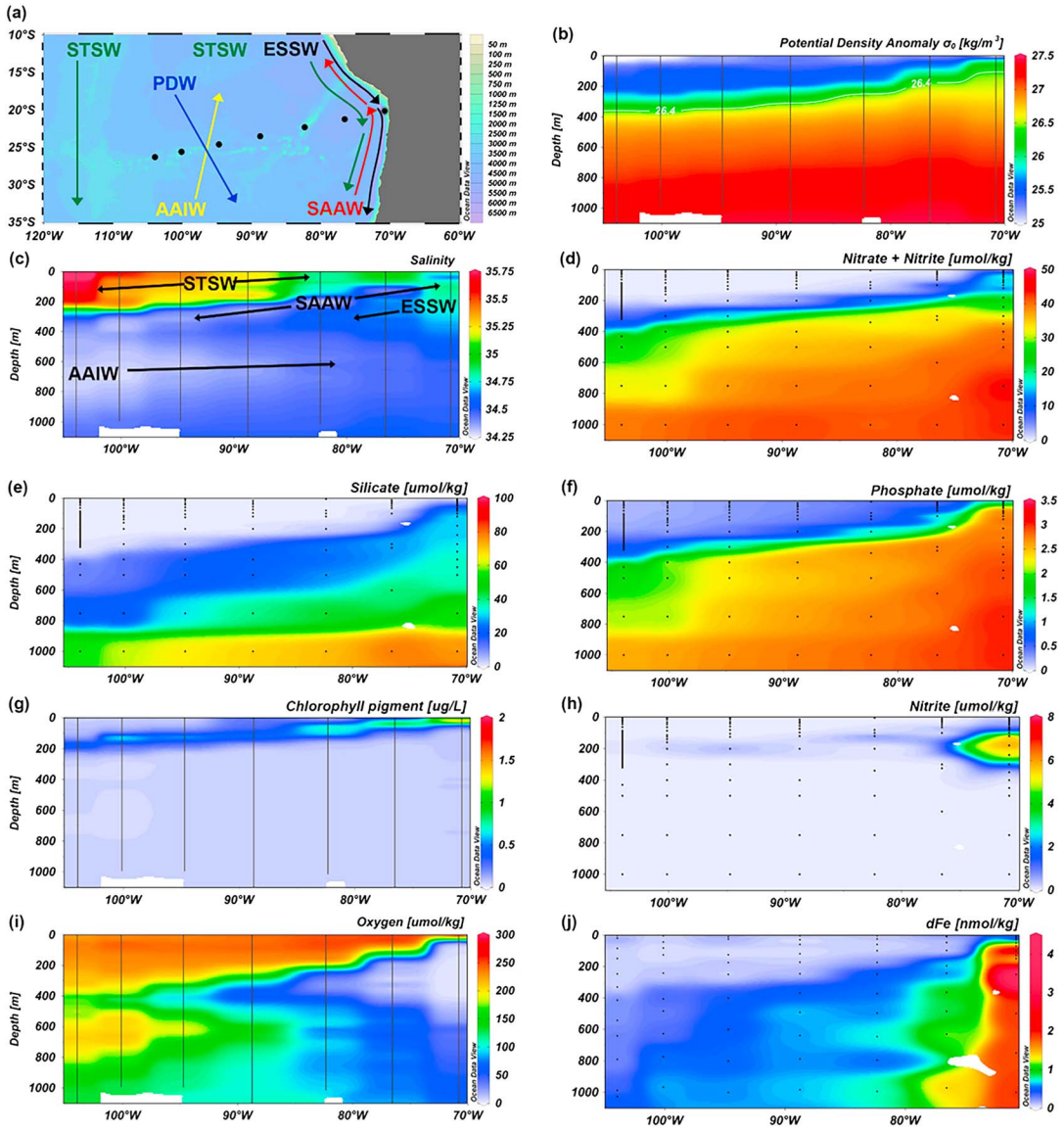


**Figure 3.** The physical circulation, hydrography, and nutrient distribution on the BiG RAPA cruise in the upper 1000 m. The seven stations are indicated with black dots (or lines) at each sampling depth. The representative water masses are taken from *Silva et al.* [2009] and *Llanillo et al.* [2013] and include Subtropical Water (STW), Equatorial Subsurface Water (ESSW), Subantarctic Water (SAAW), Antarctic Intermediate Water (AAIW), and Pacific Deep Water (PDW).

reduced Mn(II) and Fe(II), can be supplied, maintained, and transported into ODZ waters due to the fact that the ODZ water column impinges on the anoxic sediment-water interface [*Scholz et al.*, 2014]. Thus, chemical gradients across the Southeast Pacific ODZ are maintained both by in situ water column and laterally advected sediment redox processes.

The Southeast Pacific ODZ is the fourth largest of all ODZs [*Helly and Levin*, 2004], constituting ~11% of global ODZ spatial extent. The vertical extent (thickness) of the ODZ reaches 700 m off of Peru near 10°S and horizontally extends >7000 km offshore [*Fuenzalida et al.*, 2009]. Further south off Chile near 20°S, where the ODZ Station 1 of this study was sampled, the ODZ is thinner (200–300 m thick) and extends only ~1000 km offshore (Figure 3). Nanomolar traces of both oxygen and hydrogen sulfide, as well as the presence of sulfate-reducing and sulfide-oxidizing bacteria, show the potential for this ODZ to reach in situ anoxia [*Ulloa et al.*, 2012]. Station 1 of this study was positioned 80 km off of the Chilean coast, which is beyond the narrow ~10 km continental shelf, in ~1750 m depth of water. Here the ODZ extends from 100 to 400 m depth and reaches oxygen concentrations $\leq$2 μmol/kg (Figure 3). Coincident with the observed ODZ was a

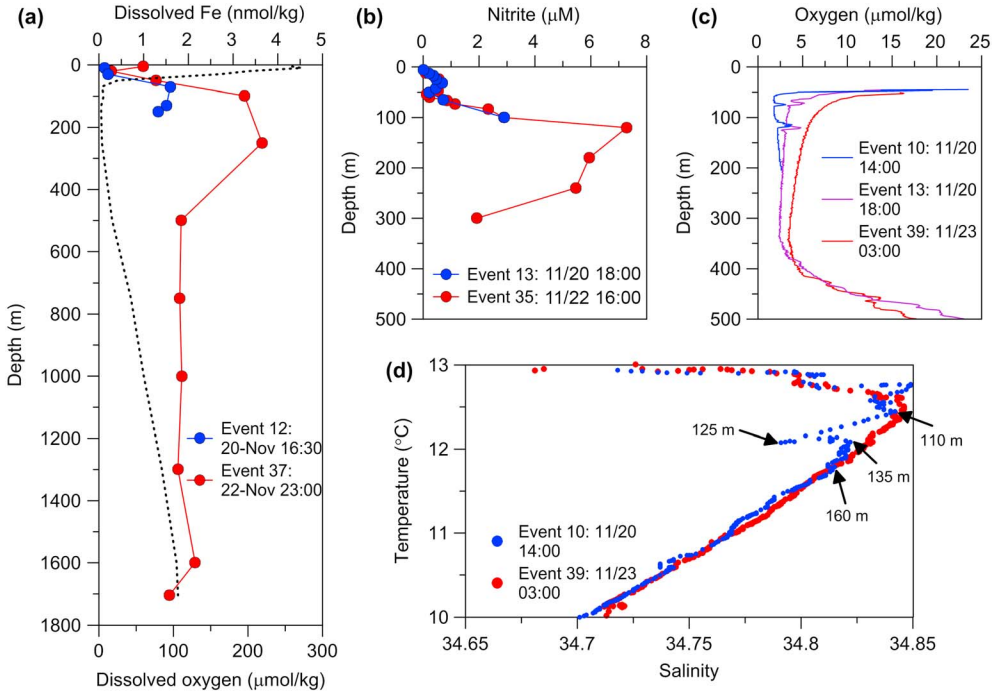


**Figure 4.** Time series of (a) dissolved Fe, (b) nitrite, (c) oxygen, and (d) temperature-salinity at Station 1. Though not all parameters were measured on a single cast, the time/date of each cast is indicated, and casts closely linked in time are grouped by color. Dissolved Fe had highest concentrations in the ODZ core. The dissolved Fe concentration in the upper ODZ changed by nearly a factor of 2 in 2 days. Redox-sensitive nitrite did not appear to change by the same factor (Figure 4b), while oxygen did (Figure 4c), though opposite to redox expectations. However, the excursion of the temperature-salinity plot (Figure 4d) around 125 m depth shows that an excursion to a different water occurred at the depth of interest over the 2 days when samples were taken for dissolved Fe, and these may have carried different dissolved Fe loads.

strong nitrite maximum (>6 μM) from 100 to 300 m depth, indicating a clear redox transition in the water column from oxic to reducing conditions.

Dissolved Fe concentrations at Station 1 were elevated to 0.99 nmol/kg at the surface, dropped to a minimum of 0.12–0.28 nmol/kg between 10–30 m, and reached a maximum of 3.65 nmol/kg at 250 m in the ODZ (Figure 3). In previous studies it was shown that only over wide continental shelves (e.g., ~150 km width, off of northern Peru) is there sufficient deposition of both lithogenic Fe and organic matter to provide a constant source of reductively mobilized Fe(II) into the water column [*Bruland et al.*, 2005]. In fact, *Scholz et al.* [2011] reported porewater Fe concentrations of up to 35 μmol/kg along the wide continental shelf near 11°S, and porewater fluxes of Fe along these shelves were as high as 88 mmol $m^{-2}$ $yr^{-1}$. Accordingly the upwelled seawater overlying the wide Peruvian shelves has been found to have extremely high dFe concentrations of >50 nmol/kg [*Bruland et al.*, 2005]. Narrow continental shelves, in contrast, do not have sufficient Fe flux from porewaters because there is insufficient shelf width for organic matter and lithogenic Fe to accumulate [*Bruland et al.*, 2001; *Bruland et al.*, 2005], keeping surface dFe concentrations in overlying seawater low. This is exemplified by the comparatively low ~1 nmol/kg dFe observed at the surface of Station 1 where the shelf is only ~10 km wide. The subsurface dFe minimum at 10–30 m coincides exactly with the chlorophyll maximum (Figure 3), which reached chlorophyll concentrations >1.5 μg/L, indicating biological utilization of dFe at these depths.

The maximum dFe values of ~3.65 nmol/kg observed at Station 1 were coincident with the lowest oxygen concentrations, ≤2 μmol/kg, in the 100–400 m depth ODZ range (Figure 4). This dFe matches the 3.3 nmol/kg dFe measured in the ODZ off the Chilean coast further south near 35°S (Figure 6) [*Blain et al.*, 2008] and 2–5 nmol/kg dFe measured within the ODZ further north off Peru near 6°S [*Chever et al.*, 2015], indicating that similar dFe concentrations are likely common throughout the southern Peruvian and Chilean ODZs. Observations over wide continental shelves have recorded ODZ dFe concentrations of 50–120 nmol/kg emanating from the sediments [*Bruland et al.*, 2005], with about half of this dFe in the reduced Fe(II) form [*Hong and*

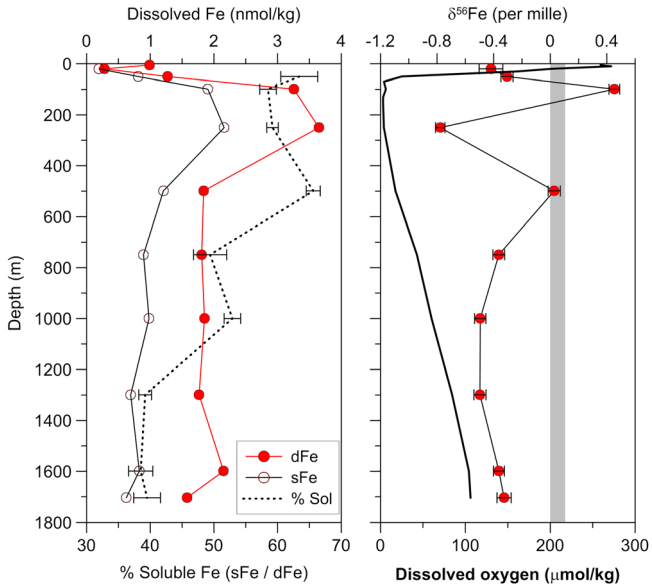


**Figure 5.** Dissolved Fe size partitioning and Fe isotopes at the ODZ Station 1. The percent of dissolved Fe composed of soluble-sized species is shown as the dotted line, with propagated error bars indicated. Dissolved oxygen concentrations are shown as the solid black line, and the crustal $\delta^{56}$Fe value of ~0.1‰ [*Beard et al.*, 2003] is indicated by the gray bar.

*Kester*, 1986]. This is different from the Arabian Sea ODZ, where lower dFe maxima of only 1–2 nmol/kg were recorded, again with ~50% in the Fe (II) form, but the Arabian Sea dFe maxima were believed to be generated in situ by remineralization and/or denitrification and stabilized at high concentration by low dissolved oxygen concentrations (≤2 μmol/kg) in the water column [*Moffett et al.*, 2007]. While we cannot eliminate the possibility that the ~3.5 nmol/kg dFe in the ODZ at Station 1 is formed in situ, it is much more likely that this dFe is derived from sediment porewaters and mixed offshore across the ~55 km distance between the 400 m isobaths to Station 1, following the dFe distributions in the literature that illuminate a bottom source of Fe [*Bruland et al.*, 2005; *Hong and Kester*, 1986].

Additionally, if the dFe distribution and speciation along the narrow shelf region of 16–18°S off of Southern Peru is representative of our Station 1 samples near 20°S, then ≤50% of the ODZ dFe at Station 1 was in the Fe(II) form [*Vedamati et al.*, 2014]. Fe(II) would likely fall into the soluble (<0.02 μm) size fraction, while margin-derived nanoparticulate Fe that also might contribute to this dFe maximum would fall in the colloidal size fraction. As can be seen in Figure 5, the percent of dFe observed in the <0.02 μm soluble fraction increased to 60% in the ODZ, relative to the 40–50% soluble Fe above and below, consistent with a hypothesis of additional soluble-sized Fe(II) delivery to the ODZ dFe layer. However, these physical speciation data do not preclude that this additional soluble Fe is in the Fe(III) oxidation state, such as would be the case if additional soluble-sized organic Fe(III)-binding ligands [*Fitzsimmons et al.*, 2015a; *Schlosser et al.*, 2013] were supplied from the shelf, though to date benthic ligand sources have been shown to supply weaker ligands of humic composition [*Bundy et al.*, 2014], which would rather fall in the colloidal size fraction.

A second reoccupation of Station 1 approximately 2.5 days after the first sampling event allowed for the discovery of significant temporal variability in the dFe concentration (a factor of two change) over this short 2.5 day time scale (Figure 4). At first it was hypothesized that redox conditions might have changed over these 2 days, modifying the supply of soluble Fe(II). However, as can be seen in Figure 4c, the higher dFe was observed on 23 November when oxygen was higher, in contrast to redox expectations. These oxygen patterns and insignificant changes in nitrite concentrations over the two sampling dates (Figure 4b) make it unlikely that a change in redox conditions could explain the short-term temporal variability in dFe at Station 1. Upon closer investigation of the hydrography, it was observed that there was a significant salinity excursion to fresher conditions near 100–150 m on 20 November compared to 23 November, marking a change in water mass moving through Station 1 on these two dates. The slightly fresher waters on 20 November must have carried a lower dFe load than the more saline waters traveling through the same area on 22–23 November in order to explain the temporal change recorded. We note that the primary circulation in this region is meridional, and thus, waters from north or south of the study location are constantly being carried through Station 1. Previous studies along the Southeast Pacific ODZ have recorded marked changes in sediment redox conditions over short temporal and spatial scales [*Scholz et al.*, 2014] that could change the supply of Fe moving in the Humboldt Current System over short time scales. If true, these temporally variable dFe concentration data further support our conclusion that the enriched dFe in the Peruvian/Chilean ODZs is an advected feature deriving from margin processes.

The stable isotope ratio of dissolved Fe ($\delta^{56}$Fe) gives additional insight into the transformations of margin-derived Fe in the water column at Station 1. The seawater dissolved Fe isotope results from this study at Station 1 ranged from −0.78 to +0.45‰ (Figure 5). The lightest $\delta^{56}$Fe value (−0.79 ± 0.03‰) occurred at 250 m depth in the heart of the ODZ where oxygen concentrations were ≤2 μmol/kg, which appears at first glance to be consistent with a light porewater Fe(II) source, similar to the $\delta^{56}$Fe signatures of −0.3 to −1.3‰ observed in the Peruvian ODZ further North [*Chever et al.*, 2015]. Interestingly, we also observe moderately light $\delta^{56}$Fe values of −0.3 to −0.4‰ in surface waters. This suggests that light Fe sourced from sediments is also important for surface waters above the ODZ (see discussion in section 3.3). From 750 m depth through the bottom at 1750 m, the mean $\delta^{56}$Fe of −0.41 ± 0.16‰ (2 SD, $n = 5$) is also suggestive of a margin-derived reductive Fe source for deep coastal waters that is different from the heavier $\delta^{56}$Fe hydrothermal Fe source present in deep waters offshore (discussed below) and is instead more similar to the California margin-reduced Fe source inferred based on $\delta^{56}$Fe of −0.3 to −0.6‰ over a similar depth range (550–2000 m) at the SAFe Station in the North Pacific [*Conway and John*, 2015], some ~2000 km from the margin.

Two heavier $\delta^{56}$Fe values are recorded at 100 m (+0.47 ± 0.05‰) and 500 m depth (+0.01 ± 0.05‰). In the middle of these heavy values, the $\delta^{56}$Fe measured at 250 m (−0.8‰) is the lightest value measured in the entire profile and is much lighter than the values immediately above and below at 100 and 500 m depth. Such large variability over a short depth range is uncommon in the ocean and thus raises the question of whether these samples suffered from sampling artifacts or an analytical inaccuracy. To address these possibilities, we replicated extraction and analysis of Fe from separate 1 L sample aliquots from 100, 250, and 500 m depths. In all three cases, replicate analyses yielded excellent agreement (+0.48 ± 0.03‰ and +0.45 ± 0.04‰ for 100 m, −0.84 ± 0.03‰ and −0.78 ± 0.03‰ for 250 m, and −0.01 ± 0.03‰ and +0.03 ± 0.04‰ for 500 m), discounting analytical problems. We therefore have confidence that the $\delta^{56}$Fe are representative of the acidified seawater collected in our 4 L low-density polyethylene sample bottles. We also discount the likelihood that the divergent pattern in $\delta^{56}$Fe with depth resulted from sample processing in the presence of oxygen (no glove box), since every sample in the ODZ would have been similarly affected by time-sensitive oxidation reactions, and thus, it cannot explain the depth-dependent $\delta^{56}$Fe shifts.

First, we consider the very light $\delta^{56}$Fe at 250 m depth to be compromised and thus ignore it, leaving a robust ($n = 4$) linear trend of $\delta^{56}$Fe from heavier values (+0.45 ± 0.04‰) in the heart of the ODZ at 100 to isotopically light values (−0.5‰) at 1000 m depth. Heavy $\delta^{56}$Fe in the ODZ is perhaps surprising, since isotopically light $\delta^{56}$Fe between roughly −1‰ and −3.5‰ is commonly reported in the literature to arise from low-oxygen porewaters [*Rouxel et al.*, 2008a; *Severmann et al.*, 2006; *Severmann et al.*, 2010] and in seawater overlying reducing sediments [*Chever et al.*, 2015; *Conway and John*, 2014; *John et al.*, 2012]. These light $\delta^{56}$Fe result from an equilibrium redox process between Fe(II) and Fe(III), in which dissolved Fe(II) in porewaters is ~3‰ lighter than Fe(III) [*Welch et al.*, 2003].

There are several potential explanations for heavy $\delta^{56}$Fe in the ODZ. First, dFe could have been non-reductively sourced from oxic sediments nearby, which would lead to $\delta^{56}$Fe near or above (in the cast of non-reductive dissolution) crustal values [*Homoky et al.*, 2013; *Radic et al.*, 2011]. In fact, there is spatial heterogeneity in the oxidation state of the sediments along the continental shelf/slope of this region, and there is also some temporal variability in sediment oxidation state, with recorded periods of oxidizing porewater conditions in recent years [*Scholz et al.*, 2014]. With the dominant meridional transport in this region, Fe supply from more oxidized regions farther north or south along the South American margin could provide lithogenic Fe inputs to Station 1 in this way. Our second hypothesis involves an active isotope effect in which if there was sufficient sulfide produced in sediment porewaters, isotopically light FeS (s) production would result, driving the remaining Fe in solution toward heavier values [*Roy et al.*, 2012; *Severmann et al.*, 2006; *Sivan et al.*, 2011]. This could occur at an isolated depth such as 250 m, since redox processes in this shelf region are highly dynamic and spatially variable [*Scholz et al.*, 2014].

However, we have no evidence that there is any problem with the isotopically light 250 m sample, since the macronutrient and dFe concentrations fit within the profile shape collected using the other sampling system, and sampling artifacts were discounted above. We note that $\delta^{56}$Fe values of similar negative magnitude have been observed in the ODZ water column both along the California margin and the Peruvian ODZ [*Chever et al.*, 2015; *John et al.*, 2012]. It could be that the processes controlling $\delta^{56}$Fe at Station 1 vary on short temporal and depth/spatial scales, such that partial reoxidation of porewater Fe in some regions (resulting in lighter $\delta^{56}$Fe

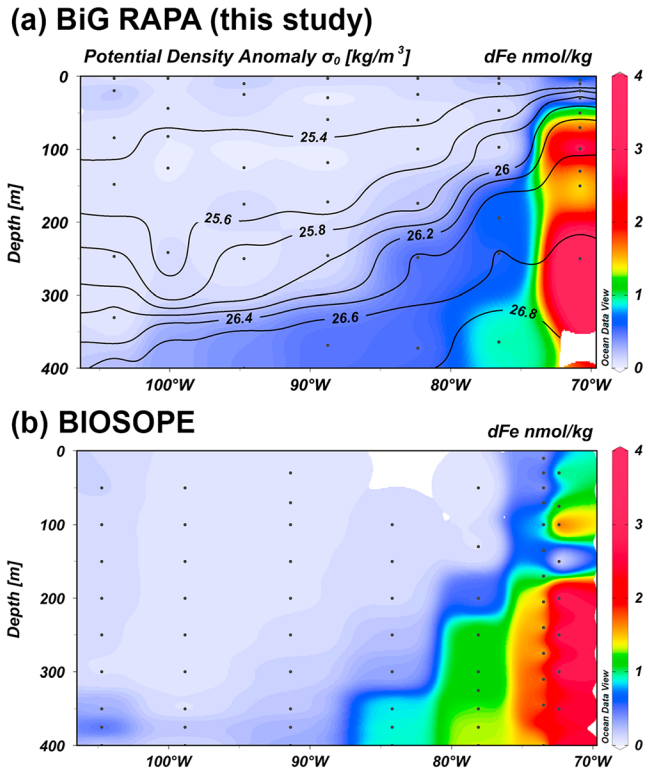


**Figure 6.** The dFe distribution (colors) in the upper 400 m of (a) the BiG RAPA transect of this study (20–27°S) and (b) the BIOSOPE transect of Blain *et al.* [2008] (28–35°S). Station locations are indicated in Figure 1.

values thereafter) influences portions of the water column offshore while in other regions near-quantitative sediment Fe dissolution or FeS precipitation dominates, creating the highly variable $\delta^{56}$Fe pattern observed. Additionally, the variability in $\delta^{56}$Fe could also be related to non-quantitative precipitation or adsorption of Fe to particles within the water column or at the sediment-water interface, the evidence and associated kinetic fractionation factors for which are quite mixed in the literature [*Scholz et al.*, 2014; *Skulan et al.*, 2002; *Staubwasser et al.*, 2013]. Further constraint of kinetic and equilibrium isotope effects occurring in seawater are required to fully understand the processes that lead to the observed $\delta^{56}$Fe variability.

To conclude, our data suggest that the Peruvian and Chilean ODZ $\delta^{56}$Fe is affected at least in part by reductive dissolution of Fe in porewaters leading to lighter $\delta^{56}$Fe than continental crust. However, we must emphasize that while the light $\delta^{56}$Fe values measured at Station 1 ($-0.3$‰ to $-0.6$‰) are lighter than crustal material ($\sim+0.1$‰ [*Beard et al.*, 2003; *Poitrasson*, 2006]), they are heavier than the porewater and seawater $\delta^{56}$Fe typically observed in low-oxygen porewaters and seawater from the California margin ($-2$ to $-3$‰ [*John et al.*, 2012; *Severmann et al.*, 2006; *Severmann et al.*, 2010]) and also heavier than would be predicted for Fe(II) in isotopic equilibrium with Fe(III) with a crustal signature [*Welch et al.*, 2003]. Our moderately light $\delta^{56}$Fe data, however, are similar to values measured elsewhere in the Peruvian ODZ: *Scholz et al.* [2014] calculated a $-0.53$‰ porewater $\delta^{56}$Fe at 11°S based on sedimentary $\delta^{56}$Fe data, and *Chever et al.* [2015] measured a $\delta^{56}$Fe of $-0.5$ to $-1.3$‰ in the water column above the Peruvian shelf at 5–6°S (station locations in Figure 1). The most likely explanation for why these values do not reach the extremely light $<-2$‰ values of the California margin is that the Southeast Pacific water column ODZ is in contact with anoxic sediments such that the reductive Fe release from sediments is near-quantitative and thus is not fractionated to lighter values during reoxidation at the sediment-water interface.

The variability with depth in these data highlights the complexity and oftentimes transient nature of Fe cycling along the South American ODZ. Such data have implications for the use of a single end-member $\delta^{56}$Fe value (or a small range in $\delta^{56}$Fe) applied to release of Fe from reductive sediments when applied to the global ocean and for mass balance calculations, as used by *Conway and John* [2014]. Instead, these data suggest that in some locations the $\delta^{56}$Fe signature of Fe effluxed to the water column might be more dependent on local processes and is thus more variable between different environments and ocean basins, complicating efforts to calculate source contributions with single end-member $\delta^{56}$Fe values.

### 3.3. Offshore/Gyre: Stations 2–7

Moving offshore into the gyre, the dFe distribution from BiG RAPA between 20 and 27°S was nearly identical from 0 to 400 m depth to that of the earlier BIOSOPE cruise at 28–35°S (Figure 6, station locations in Figure 1). Concentrations of dFe were $<0.1$ nmol/kg from the surface down to 400 m depth at the stations nearest the

**Table 2.** Vertical Diffusive Fluxes of Dissolved Fe Through the Ferricline

| Station | Pycnocline Depth (m) | Ferricline horizon (m) | $K_V$ ($m^2\ s^{-1}$) | dFe flux ($\mu mol\ m^{-2}\ yr^{-1}$) |
|---|---|---|---|---|
| 2 | 25–200 | 97 | $7.24 \times 10^{-5}$ | 7.3 |
| 3 | 160–250 | 174 | $3.37 \times 10^{-5}$ | 5.0 |
| 4 | 190–400 | 246 | $2.08 \times 10^{-5}$ | 2.1 |
| 5 | 215–400 | 250 | $3.97 \times 10^{-5}$ | 2.8 |
| 6 | 230–400 | 242 | $3.14 \times 10^{-5}$ | 1.5 |
| 7 | 215–400 | 231 | $3.17 \times 10^{-5}$ | 2.3 |

gyre center, while they had already exceeded 0.2 nmol/kg by a much shallower 200 m depth at the two stations situated in the transition between the ODZ and the gyre (Stations 2 and 3). The ferricline, or depth of greatest change in dFe concentration, followed the 26.4 $kg/m^3$ potential density layer in both transects. The similarity of these distributions, despite their spatial and temporal (6 years, similar season) differences, demonstrates that Fe dynamics are likely very stable at this distance from the margin along the entire Chilean coast.

However, the South Pacific gyre dFe concentrations of ≤0.1 nmol/kg are extremely low, even for oligotrophic regions. For example, in one portion of the North Pacific subtropical gyre at Station ALOHA, surface dFe concentrations are a higher 0.2–0.7 nmol/kg depending on seasonal atmospheric dust inputs, where a surface dFe maximum can be resolved from the dFe minimum of ~0.06 nmol/kg at 125 m depth in the deep chlorophyll maximum (DCM) [*Fitzsimmons et al.*, 2015b]. Similarly, in the North Atlantic surface dFe concentrations of 0.4–2.0 nmol/kg also result from aerosol deposition and can be distinguished from dFe minima at the ~70 m DCM [*Fitzsimmons et al.*, 2013; *Fitzsimmons et al.*, 2015c; *Sedwick et al.*, 2005]. This is different from the South Pacific oligotrophic gyre of this study, where no surface dFe maximum could be distinguished from a dFe minimum at the DCM (Figure 3), since dFe is drawn down throughout the entire euphotic zone through the 26.4 isopycnal. These data are similar but slightly more extreme than in the South Atlantic gyre, where dFe is only drawn down to a higher ≤0.2 nmol/kg through 200 m depth [*Noble et al.*, 2012].

Variable dust fluxes can explain the differences between surface dFe distributions in these oligotrophic gyre regions. For instance, dust inputs to the Southeast Pacific Ocean are some of the lowest ever observed globally, with Fe dust fluxes measured on the BIOSOPE cruise of only 1.8–2.3 $\mu mol\ m^{-2}\ yr^{-1}$ [*Wagener et al.*, 2008]. Other South Pacific dust Fe flux estimates are as low as 8.7 $\mu mol\ m^{-2}\ yr^{-1}$ [*Buck et al.*, 2013]. These fluxes are orders of magnitude lower than the rates of aerosol deposition to the North Atlantic near Bermuda of 180–10,000 $\mu mol\ m^{-2}\ yr^{-1}$ [*Sedwick et al.*, 2007] and are also lower than the fluxes of aerosol Fe to the South Atlantic inferred from models of ≥36.5 $\mu mol\ m^{-2}\ yr^{-1}$ [*Noble et al.*, 2012].

Thus, it is useful to compare these low dust fluxes in the South Pacific gyre to the vertical and horizontal fluxes of dFe to the surface ocean in order to determine which source is the major supply of dFe to South Pacific gyre microorganisms. Because dFe measurements were made to 1000 m depth in this study, vertical diffusive dFe fluxes through the ferricline (100–350 m, depending on station) were able to be calculated as the product of the vertical turbulent diffusivity coefficient ($K_V$) and $\delta$(Fe)/$\delta z$. Here $\delta$(Fe)/$\delta z$ was calculated in the ferricline of each station, which always coincided with the broad pyconocline at 100–400 m in depth. The $K_V$ term was calculated by using the potential density data for each station, following the determination by *Gargett* [1984] for stratified systems where it can be assumed that the diapycnal vertical mixing is dominated by internal wave breaking:

$$K_V = \frac{a_0}{N} \tag{1}$$

where $a_0$ is a constant differentiating oceanic waters from lake/estuarine waters and $N$, the buoyancy frequency is

$$N = \sqrt{\frac{g\ p_0}{\frac{\delta p}{\delta z}}} \tag{2}$$

where $g$ is the gravitational constant, $p_0$ is the potential density at a given depth, and $\delta p/\delta z$ is the change in potential density across a given depth interval, in this case the depth horizon within the pycnocline across which Fe is being transferred (top of the ferricline). The calculated $K_V$ values are summarized in Table 2

**Table 3.** Horizontal Turbulent Fluxes of Dissolved Fe Between the Base of the Mixed Layer (MLD) and 250 m Depth (Top of the Ferricline)[a]

| Station | MLD (m) | Distance From Station 1 (km) | dFe flux ($\mu$mol m$^{-2}$ yr$^{-1}$) |
|---|---|---|---|
| 2 | 20 | 620 | 127,000 |
| 3 | 23 | 1,225 | 67,500 |
| 4 | 60 | 1,900 | 33,400 |
| 5 | 43 | 2,512 | 17,700 |
| 6 | 33 | 3,067 | 9,940 |
| 7 | 30 | 3,454 | 6,640 |

[a] $K_H = 5520$ m$^2$/s was calculated by using the dFe gradient and the parameterization of *Okubo* [1971].

and are nearly identical to the values measured in the Southern and Atlantic Oceans of $3 \times 10^{-5}$ m$^2$ s$^{-1}$ [*Ledwell et al.*, 1998; *Loscher et al.*, 1997].

The vertical diffusive fluxes through the pycnocline/ferricline and into the near-surface waters of the South Pacific gyre ranged from 1.5 to 7.3 $\mu$mol m$^{-2}$ yr$^{-1}$ and are summarized in Table 2. There is a generally decreasing diffusive flux moving offshore, although within the gyre (Stations 4–7) the diffusive vertical dFe fluxes are nearly constant within error. To compare these values to the dust-derived Fe fluxes measured in the South Pacific of 1.8–8.7 $\mu$mol m$^{-2}$ yr$^{-1}$, a 10% aerosol Fe solubility in seawater was applied conservatively, which is on the high end of 0.5–10% solubility reported in the literature for dusts of varying origin [*Buck et al.*, 2013; *Sedwick et al.*, 2007]. This results in an estimated dust-derived Fe flux of 0.2–0.9 $\mu$mol m$^{-2}$ yr$^{-1}$, which is lower than all of the vertical diffusive Fe fluxes reported in Table 2. Thus, the surface-dissolved Fe in the South Pacific gyre appears to be dominated by oceanic Fe sources, not external Fe sources such as dust.

How does this compare to the horizontal dissolved Fe flux from the margin/ODZ? The amount of dFe transported from the margin would depend on lateral diffusive fluxes and/or the presence of zonal circulation pathways. As described above, the STW, ESSW, and SAAW all have predominantly meridional flow (Figure 3), which forms an advective barrier between Station 1 and the rest of the stations of the transect. However, there do appear to be bands of zonal advective transport mediated by eddies in the South Pacific at Peruvian latitudes [*Czeschel et al.*, 2011], though these have not been described for the Chilean latitudes of this study.

We calculated the horizontal turbulent flux of Fe ($F_H$ in $\mu$mol/m$^2$/yr) at depths from the base of the mixed layer to 250 m, which is the top of the ferricline for most stations (Table 2), using the following equation:

$$F_H(x) = K_H \frac{\partial \mathrm{Fe}(x)}{\partial x} \tag{3}$$

where $x$ is the distance from Station 1, $K_H$ is the horizontal turbulent diffusivity (in m$^2$/s), and $\partial$Fe/$\partial x$ is the gradient in dFe concentrations along the transect from Station 1. An exponential dependence of dFe concentrations on distance from shore indicates the dominance of eddy diffusive mixing, and thus, the data were fit to the exponential function:

$$\mathrm{Fe}(x) = \mathrm{Fe}_0 e^{-x/D} \tag{4}$$

where $\mathrm{Fe}_0$ is the dFe concentration at Station 1 and $D$ is the distance over which dFe concentrations decrease to 1/$e$ of their initial value [*Rijkenberg et al.*, 2012]. Dissolved Fe data between the base of the mixed layer and the top of the ferricline (typically ~250 m depth) were used in this calculation, with an $\mathrm{Fe}_0$ of 1.2 nmol/kg and a resulting $D$ of 962 km ($R^2 = 0.44$; Figure S1 in the supporting information). This $D$ can be used to calculate $K_H$ (in cm$^2$/s by the parameterization of *Okubo* [1971]:

$$K_H = 0.103 l^{1.15}$$

where $l = 3D$ in centimeter.

The calculated horizontal eddy turbulent fluxes of dFe ranged from 6640 $\mu$mol/m$^2$/yr at the most western Station 7 to 127,000 $\mu$mol/m$^2$/yr at Station 2 (Table 3). These fall within the same range as the lateral dFe fluxes calculated by *Rijkenberg et al.* [2012] off the NW African margin. Importantly, however, these horizontal dFe fluxes were 3 orders of magnitude greater than the vertical diffusive fluxes across the ferricline (1–7 $\mu$mol/m$^2$/yr; Table 2) and dust fluxes (<1 $\mu$mol/m$^2$/yr) to the surface ocean, making lateral dFe supply the most important source of dFe to gyre phytoplankton by far.

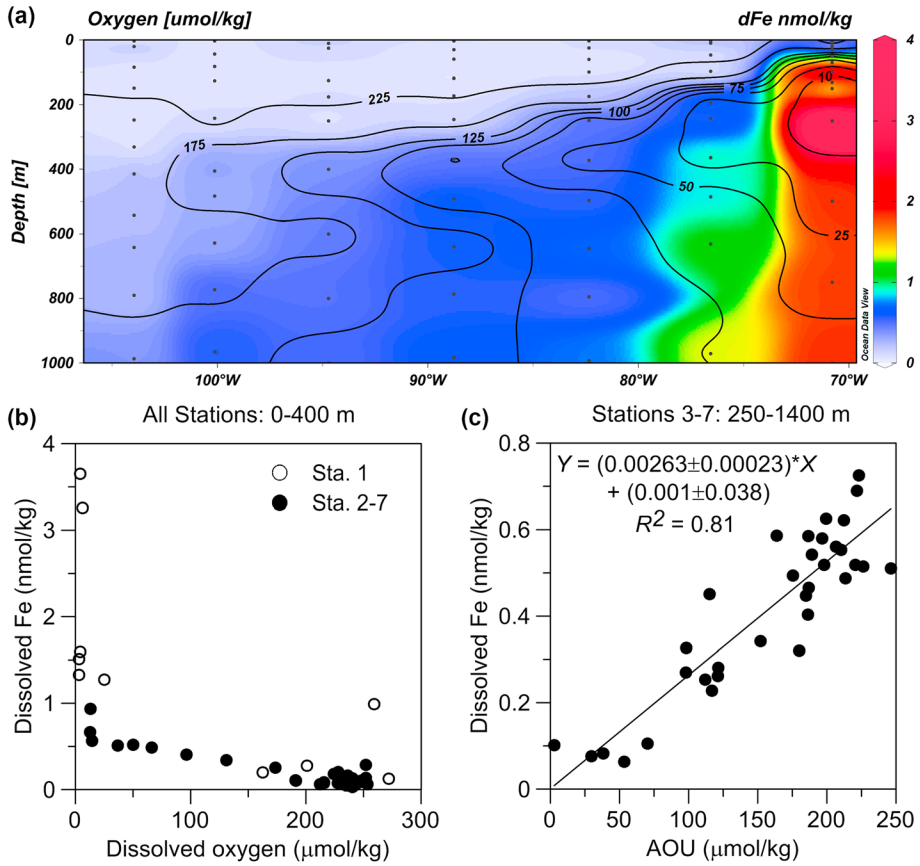


**Figure 7.** Relationships between dFe and oxygen. (a) Dissolved Fe distributions are shown in color, while dissolved oxygen is shown with black contour lines. (b) Dissolved Fe in the upper 400 m of the entire transect is dependent on oxygen, with Fe(II) stabilized at high concentrations at oxygen <25 μmol/kg. (c) The strong relationship between dissolved Fe and AOU from 250 to 1400 m depth in the gyre indicates that remineralization is the main source of dFe to these waters.

To evaluate whether this shelf Fe could be in the reduced Fe(II) form, we also evaluated the potential control of dissolved oxygen concentrations on offshore dFe transport (Figure 7a). From this, it can be seen that elevated dFe concentrations were observed only when oxygen was <25 μmol/kg, most likely resulting from dFe stabilization as Fe(II) in the absence of oxygen, as discussed above. However, this was only true for Station 1 and a few depths of Station 2 (Figure 7b), indicating that Fe(II) species likely do not make it very far offshore from the margin, in accordance with prior studies [e.g., *Vedamati et al.*, 2014].

In contrast, from Station 3 offshore into the gyre at depths >250 m (below the ferricline), dFe had a direct relationship with apparent oxygen utilization (AOU; Figure 7c), which is a measure of the amount of oxygen consumption in a water parcel due to biological remineralization since that water parcel was last in contact with the atmosphere. A correlation between dFe and AOU is an indication that remineralization is the main source of dFe to these deeper, offshore waters. The dFe/AOU slope of this line was converted to a dFe:C ratio using the AOU:C ratio of 1.6 [*Martin et al.*, 1987]. The resulting dFe:C ratio of 4.2 μmol/mol is slightly higher than the 1.6–2.4 μmol/mol ratios found in the Fe-limited equatorial Pacific and Southern Ocean regions [*Sunda*, 1997] but is within the range of 2.6–4.4 μmol/mol measured in the N-limited, oligotrophic North Pacific [*Martin et al.*, 1989; *Martin et al.*, 1993]. These dFe:C ratios are much lower than the 6–11 μmol/mol ratios measured in the Fe replete, "dusty" North Atlantic [*Bergquist and Boyle*, 2006; *Fitzsimmons et al.*, 2013; *Hatta et al.*, 2015]. Thus, based on the dFe:C ratios we found in this study, phytoplankton production in the Southeast Pacific gyre is not likely generally limited by dFe. However, while $N_2$ fixers are typically limited by Fe and/or P, based on the ≥0.2 μmol/kg P concentrations (Figure 3), Fe likely controls diazotroph activity in this region. While earlier incubation studies did not show a response to Fe additions [*Bonnet et al.*, 2008], it is possible that dFe concentrations were so low that there was an insufficient seed population of

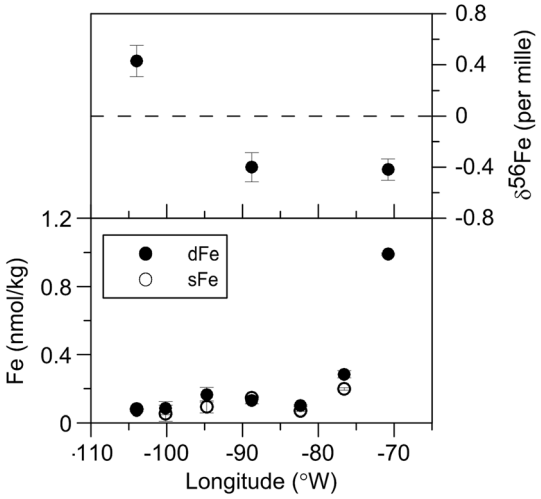


**Figure 8.** (top and bottom) Dissolved Fe concentrations, size partitioning into soluble/colloidal fractions, and Fe isotope ratios in the surface mixed layer. The error bars in Figure 8 (top) show the 2$\sigma$ internal errors, while the error bars in Figure 8 (bottom) show 1 SD on replicate analyses of each sample.

diazotrophs to produce a short-term response to Fe additions in incubation experiments. Given the low dFe concentrations in euphotic zone waters (Figure 7), recycling of Fe must be an important pathway of Fe provision to surface microorganisms.

### 3.4. Offshore-Dissolved $\delta^{56}$Fe

As discussed in section 3.2, the stable isotope ratio of dFe in seawater ($\delta^{56}$Fe) is a useful tool for illuminating the contribution of Fe supplied by different sources with unique end-member Fe isotope signatures. It is thought that the $\delta^{56}$Fe signature of reduced Fe effluxing from the sediment-water interface is isotopically light ($-0.5$ to $-4$‰), calculated to be $-0.53$‰ off of Peru [*Scholz et al.*, 2014], while in contrast, Fe released from sediments via nonreductive mechanisms has a $\delta^{56}$Fe of +0.2 to +0.4‰ [*Homoky et al.*, 2013]. Similarly, while dust particles individually [*Beard et al.*, 2003; *Mead et al.*, 2013; *Waeles et al.*, 2007] have a near-crustal +0.1‰ signature [*Beard et al.*, 2003; *Poitrasson*, 2006], the marine dFe solubilized from dust may be significantly heavier (+0.4 to +0.7‰), a hypothesis based primarily on the pervasive heavy $\delta^{56}$Fe patterns in the North Atlantic that presumably results from nonreductive dust Fe dissolution and/or binding by organic ligands [*Conway and John*, 2014]. Thus, by using the $\delta^{56}$Fe signatures of end-member Fe sources such as these, the relative contribution of various Fe sources to the ocean can be revealed.

The surface ocean is an important place to investigate Fe sources, since this is the region where relative Fe supply has the greatest effect on primary production. The most likely potential sources of Fe to the surface Southeast Pacific include dust deposition, reduced Fe from shelf porewaters, nonreductive Fe release from margin sediments, and dFe mixing/upwelling from pycnocline seawater below. The surface $\delta^{56}$Fe values at Stations 1 and 4 were both $-0.4$‰, while at Station 7 $\delta^{56}$Fe was +0.4‰ (Figure 8). The very light $\delta^{56}$Fe at Station 1 is consistent with a reduced Fe source from the continental margin, which is perhaps unsurprising given the magnitude of dFe concentrations at the surface of Station 1 (~1 nmol/kg) compared to the other stations ($<$0.3 nmol/kg) and the proximity of Station 1 to the continental shelf. The equivalently light surface water at Station 4, which is $>$1850 km away from the South American coast, supports the large magnitude of our lateral dFe flux estimates (Table 3). These results are also consistent with the $\delta^{56}$Fe record at the SAFe station in the North Pacific, where it was suggested that light $\delta^{56}$Fe ($-0.55 \pm 0.06$‰ between 500 and 2000 m depth) sourced from low-oxygen Californian sediments is transported ~2000 km offshore from the North Pacific ODZ [*Conway and John*, 2015].

If the measured $\delta^{56}$Fe is taken to represent a primary source signature, the heavy $\delta^{56}$Fe of +0.4‰ at Station 7 can only come from two sources: mixing from below or dust input from above. The flux calculations provided in section 3.3 suggest a greater influence from Fe sources below than above; however, as Figure 9 shows, $\delta^{56}$Fe becomes lighter with depth at Station 7, inconsistent with the provision of a heavy $\delta^{56}$Fe source to the surface. Instead, the heavy $\delta^{56}$Fe surface data suggest an influence of dust in supplying the $\leq$0.1 nmol/kg dFe inventory in the gyre. Dust fluxes are known to be very low in this region [*Wagener et al.*, 2008], and since they are derived from marine sources (see Hybrid Single-Particle Lagrangian Integrated Trajectory HYSPLIT back trajectories in Figure S2 [*Draxler and Rolph*, 2014]) they have very low Fe loadings [*Buck et al.*, 2013]. However, the dFe at all gyre stations was partitioned almost entirely into the smallest soluble Fe size fraction ($<$0.02 μm; Figure 8), while high-dust regions tend to have dFe dominated $\geq$80% by colloidal-sized Fe (0.02–0.4 μm [*Fitzsimmons and Boyle*, 2014; *Fitzsimmons et al.*, 2015c]), inconsistent with dust being the dominant Fe source.

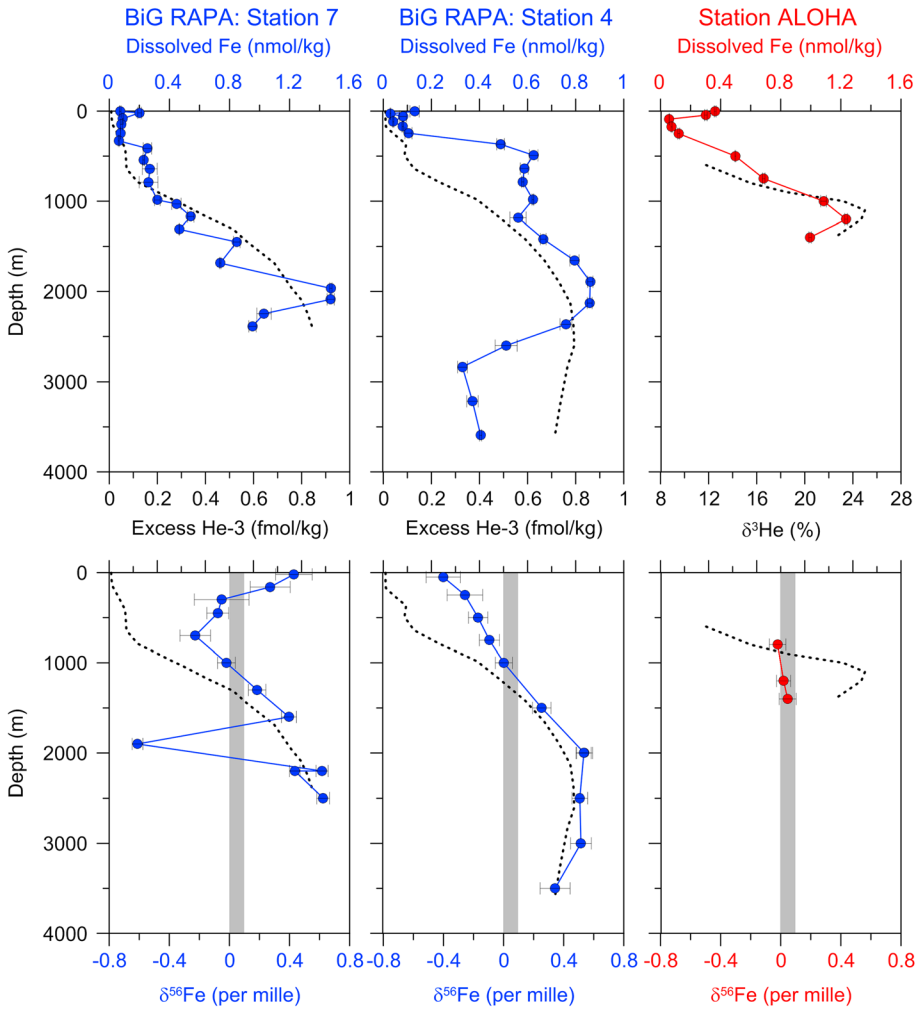


**Figure 9.** Dissolved Fe concentration and $\delta^{56}$Fe data for BiG RAPA Stations 7 and 4 (in blue, November–December 2010) in the South Pacific subtropical gyre and Station ALOHA (in red, 18 November 2012) in the North Pacific subtropical gyre. The depths where hydrothermal fluids contribute significantly to the Fe profiles are indicated by maxima in $\delta^{3}$He and excess hydrothermal He-3 data, shown as the dotted lines. The $\delta^{56}$Fe of the continental crust is indicated with the gray bar in each panel for reference [*Beard et al.*, 2003].

Thus, a simple explanation for the +0.43 ± 0.12‰ $\delta^{56}$Fe at the surface of Station 7 is a mixture of dust-derived dFe with a heavier $\delta^{56}$Fe (~ + 0.7‰ [*Conway and John*, 2014]) and dFe mixed/upwelled from the subsurface with a $\delta^{56}$Fe ≤0‰. That said, we cannot rule out a biological Fe isotope effect that might have left the surface $\delta^{56}$Fe at Station 7 isotopically heavy when the light Fe isotopes were consumed biologically, a process that has previously been documented for small phytoplankton and also inferred from water column $\delta^{56}$Fe data in the equatorial Pacific [*Ellwood et al.*, 2014; *Radic et al.*, 2011]. However, at present, evidence in the literature for such a biological fractionation is both limited and mixed, with diatoms not observed to fractionate Fe, and dissolved $\delta^{56}$Fe profiles from the North Atlantic showing no obvious evidence of biologically-driven fractionation toward heavier values [*Conway and John*, 2014; *Ellwood et al.*, 2014].

Below the surface, the ferricline occurs between 300 and 400 m depth at both Stations 4 and 7 (Figures 7 and 9), which overlaps with the depth where South Pacific waters transition from SAAW to AAIW (Figure 2). AAIW forms in the Southeast Pacific just north of the Subantarctic Front (near 60°S) at potential density 27.05–27.15 kg/m$^3$, a potential temperature of 4–6°C, and a salinity of 34.1–34.5 [*Talley et al.*, 2011]. As the OMPA model results in Figure 2 show, AAIW was the dominant water mass at 500–800 m depth at BiG RAPA Station 7. At 700 m depth at this station, there was a distinct minimum in Fe isotope ratios of −0.23 ± 0.10‰ (dFe = 0.27 nmol/kg) that coincided with the relatively freshly formed AAIW core (>80% AAIW by OMPA). At Station 4, the $\delta^{56}$Fe at

500 m depth (65% AAIW and 29% ESSW) was $-0.17 \pm 0.06$‰. The dFe concentration was higher at the AAIW depths of Station 4 than at Station 7, ~0.6 nmol/kg compared to 0.27 nmol/kg, fulfilling expectations that AAIW forms with low dFe concentrations and then receives additional dFe inputs during water mass mixing and/or remineralization along the AAIW flow path.

Thus, dFe in the AAIW layer has two likely sources: preformed dFe present in AAIW during formation and the dFe added to AAIW during water mass mixing, remineralization, or other dFe inputs along its path length. The 60 μmol/kg decrease in oxygen concentrations between the AAIW core at Stations 7 and 4 indicates that significant remineralization and/or input from the ODZ occurred between these stations that would have added dFe to these waters by the relationship in Figure 7c. However, the $\delta^{56}$Fe values between these two stations were identical within error, averaging -0.20 ± 0.24‰ (2 SD). Thus, the regenerated/ODZ dFe sourced to these waters must have had the same Fe isotope composition as the AAIW dFe. Regardless, the $\delta^{56}$Fe of $-0.20 \pm 0.24$‰ is representative of relatively newly formed AAIW in the Southeast Pacific and is not significantly eroded on a zonal scale. Although direct $\delta^{56}$Fe data from AAIW Antarctic source regions are not yet published, the isotopically light $\delta^{56}$Fe in AAIW observed in this study ($-0.20$‰) corresponds precisely with $\delta^{56}$Fe measured in samples collected from the depths of AAIW at ~31°S in the Atlantic in both 2008 and 2010 ($-0.17 \pm 0.07$‰ and $-0.18 \pm 0.09$‰ [*Conway et al.*, 2016; *Lacan et al.*, 2008]). Taken together, these observations suggest that AAIW is carrying an isotopically light preformed $\delta^{56}$Fe signature northwards or that similar internal biogeochemical processes occur as the water mass moves northward in both ocean basins.

This characterization of "end-member" AAIW $\delta^{56}$Fe can be used to interpret the source of additional dFe to AAIW waters during circulation. Two data sets containing $\delta^{56}$Fe data from AAIW in the tropical Southwest Pacific show $\delta^{56}$Fe of +0.06 to +0.44‰ across four stations [*Labatut et al.*, 2014; *Radic et al.*, 2011]. These AAIW samples are aged and eroded compared to the BiG RAPA AAIW layer, which is demonstrated by their higher salinity of 34.5, relative to a starting salinity of ~34.1–34.2 for AAIW. The dFe concentrations at these stations are much higher than those of BiG RAPA as well, ranging from 0.92 to 1.41 nmol/kg, indicating dFe inputs from remineralization and/or sediment inputs from the Papua New Guinea margin. Given that the oxygen concentration did not change significantly between BiG RAPA and the Southwest Pacific stations, a sediment-derived source of dFe is a more likely explanation of the $\delta^{56}$Fe in this region. If a $\delta^{56}$Fe of $-0.20$‰ and a dFe concentration of 0.27 nmol/kg is taken as the original AAIW end-member, then the published $\delta^{56}$Fe measured in seawater in the tropical Southwest Pacific would require a $\delta^{56}$Fe ranging from +0.12 to +0.59‰ coming from the Papua New Guinea margin. This compares well to the $+0.22 \pm 0.18$‰ signature of dFe measured for nonreductive Fe release from sediments [*Homoky et al.*, 2013], the hypothesized source of dFe from the Papua New Guinea region.

### 3.5. Hydrothermal-Dissolved $\delta^{56}$Fe: North and South Pacific Comparison

Below the AAIW layer, dFe concentrations rose to a maximum of 1.47 nmol/kg at Station 7 and 0.86 nmol/kg at Station 4 near 2000 m depth (Figure 9). The coincident rise of mantle-derived He-3 indicates that this dFe maximum was derived from East Pacific Rise (EPR) hydrothermal venting [*Fitzsimmons et al.*, 2014]. Stations 7 and 4 are 800 and 2400 km, respectively, to the east of the EPR, along southeastward flowing abyssal circulation paths (shown in Figure 3). With the exception of a single $\delta^{56}$Fe of $-0.61 \pm 0.04$‰ at 1900 m at Station 7 (discussed separately below), the $\delta^{56}$Fe of dFe in the hydrothermally influenced samples of both stations similarly increased to a maximum of $+0.56 \pm 0.11$‰ ($n = 3$; 2 SD) at Station 7 and $+0.52 \pm 0.02$‰ ($n = 4$; 2 SD) at Station 4, coincident with the respective dFe concentration maxima.

While no measurements of the native hydrothermal vent fluid $\delta^{56}$Fe in the southern EPR vents of this study have been measured, all vent fluids measured to date along both the northern EPR and the Mid-Atlantic Ridge have $\delta^{56}$Fe <0‰, ranging from $-0.21$ to $-0.69$‰ [*Bennett et al.*, 2009; *Rouxel et al.*, 2008b; *Rouxel et al.*, 2016; *Severmann et al.*, 2004]. Together with the fact that altered basalts in the high-temperature hydrothermal reaction zone have been recorded to have heavier $\delta^{56}$Fe of up to +1.3‰ [*Rouxel et al.*, 2008b], it has been hypothesized that light Fe isotopes are preferentially leached during hydrothermal vent fluid generation. This would suggest that the heavy $\delta^{56}$Fe values recorded in the downstream hydrothermal plume of this study have most likely been altered compared to EPR vent fluids, either during mixing of vent fluids with abyssal seawater in the hydrothermal plume or during transport of Fe away from the EPR.

Fractionation of Fe isotopes can occur during several possible chemical transformations of Fe from the original vent fluids to the dissolved Fe stabilized in seawater. First, during Fe sulfide precipitation, a kinetic Fe isotope effect of +0.60‰ drives the dissolved Fe(II) to heavier $\delta^{56}$Fe values relative to the light-precipitated Fe sulfide [*Bennett et al.*, 2009]. The effect of this reaction on seawater $\delta^{56}$Fe depends on vent chemistry, such as the availability of $H_2S$ versus Fe in vent fluids. For example, light $\delta^{56}$Fe unaffected by sulfide precipitation is observed in seawater-dissolved hydrothermal Fe sourced from low-sulfur vents on the Mid-Atlantic Ridge [*Conway and John*, 2014; *Severmann et al.*, 2004]. Second, oxidation of the remaining $Fe(II)_{(aq)}$ to $Fe(III)_{(aq)}$ has an associated 3‰ isotope effect that drives the Fe(III) to heavier values [*Johnson et al.*, 2002]. Third, if vent fluid Fe(II) is completely oxidized to Fe(III) that then undergoes Fe(III) precipitation, then the fractionation is dependent on precipitation rate instead of redox-associated fractionation. If precipitation is rapid, the dissolved phase can be driven to heavier $\delta^{56}$Fe values [*Skulan et al.*, 2002]. Alternatively, if oxidation of Fe(II) to Fe(III) occurs during mixing with oxic abyssal seawater while Fe(III) precipitation is occurring more slowly, this may drive Fe(II) in solution to lighter values, leaving precipitated Fe (III) isotopically heavy [*Bullen et al.*, 2001; *Welch et al.*, 2003]. From these it can be considered that the $\delta^{56}$Fe signature of hydrothermal Fe released from vents is likely dependent not only on the initial vent chemistry but also on the extent and time scale of subsequent reactions that occur upon contact with oxic-seawater and within the local hydrothermal plume, all of which may influence the far-field signature that can be observed within the ocean [*Rouxel et al.*, 2016]. Furthermore, if organic ligands bind and stabilize hydrothermal Fe(III) remaining in solution, this could result in an equilibrium isotope effect that would concentrate heavy Fe isotopes in the strongest Fe-ligand complexes [*Morgan et al.*, 2010], with the unbound Fe(III) presumably lost to precipitation.

Thus, the heavy $\delta^{56}$Fe values of $+0.54 \pm 0.14$‰ (2 SD) recorded in this study in the distal hydrothermal plume provide us with new information about chemical mechanisms of hydrothermal Fe transport from the EPR. First, the dFe is likely not in a nanoparticulate pyrite form, which would be expected to have $\delta^{56}$Fe values lighter than vent fluid [*Bennett et al.*, 2009], which we suggest is likely $<$0‰ [*Rouxel et al.*, 2008b; *Rouxel et al.*, 2016]. Colloidal pyrite (nanopyrite) formation [*Gartman et al.*, 2014; *Yucel et al.*, 2011] is one of two potential mechanisms for how dFe might escape precipitation and become stabilized in hydrothermal plumes, an observation that has come to be known as the leaky vent hypothesis [*Toner et al.*, 2012]. Second, this means that the excess colloidal Fe concentrations measured at Station 7 that were transformed into soluble Fe by Station 4 (discussed in *Fitzsimmons et al.* [2014]) are not likely to have occurred by solubilization of colloidal nanopyrite.

The other proposed mechanism of dFe stabilization in "leaky vent" hydrothermal plumes is the stabilization of oxidized Fe(III) or colloidal Fe(III)-oxyhydroxides through the binding of organic ligands [*Hawkes et al.*, 2013; *Sander and Koschinsky*, 2011], and this mechanism would be consistent with the heavier $\delta^{56}$Fe values ($+0.54 \pm 0.14$‰; 2 SD) recorded in the southern EPR plume. Sulfide precipitation and subsequent oxidation of any remaining $Fe(II)_{aq}$ would have enriched the Fe isotope signature of the dFe to values $>$0‰, and ligand binding by strong ligands could further enrich the dFe $\delta^{56}$Fe to the values recorded here. In addition, the fact that the hydrothermal $\delta^{56}$Fe at Stations 4 and 7 were not significantly different would suggest that any ligand exchange occurring between these stations did not act to fractionate $\delta^{56}$Fe significantly. Thus, the ligands participating in ligand exchange between these sites could not have had significantly different binding strength, since stronger ligands are thought to bind heavier Fe isotopes via an equilibrium isotope effect [*Morgan et al.*, 2010]. Moreover, since the contribution of background "abyssal" dFe also changed between these two stations from $<$40% at Station 7 to $\geq$50% at Station 4, the $\delta^{56}$Fe of the "abyssal background" dFe mixing with these hydrothermal end-members must also have been rather isotopically heavy. There is not sufficient non-hydrothermal abyssal $\delta^{56}$Fe data in the South Pacific to confirm or deny this inference, although North Pacific waters $>$2000 m depth did have a $\delta^{56}$Fe near 0‰ [*Conway and John*, 2015].

However, the single light $\delta^{56}$Fe value of $-0.61 \pm 0.04$‰, recorded at the Station 7 dFe concentration maximum of 1.47 nmol/kg at 1900 m depth, must be considered. This datum could be untrustworthy, similar to the 250 m value at Station 1, since it stands alone in the profiles as the only hydrothermal-influenced sample with a light $\delta^{56}$Fe value and an ~1‰ $\delta^{56}$Fe difference from the flanking samples. However, the measured $\delta^{56}$Fe was replicated by two separate chemical extractions of the same sample bottle ($-0.61 \pm 0.03$ and $-0.61 \pm 0.04$‰), and its dFe and macronutrient concentration are consistent with that of flanking samples

collected with the other sampling system, and thus, the datum is not the result of an analytical artifact nor obvious sampling contamination. As with Station 1, while we cannot entirely rule out some artifact from sampling, there is no obvious reason to discount it based on other parameters. Potential explanations for the light $\delta^{56}$Fe point include fresh hydrothermal venting of isotopically light dFe from a nearby, heretofore undiscovered hydrothermal vent along the Sala y Gomez Ridge [*Fitzsimmons et al.*, 2014]. Alternatively, that sample could be carrying an excess of isotopically depleted Fe(II) after pyrite precipitation or oxidation/precipitation of Fe(III), which would also point to recent venting, since the half-life of Fe(II) in these South Pacific waters is on the order of 2 h [*Field and Sherrell*, 2000]. Overall, if this datum is representative of the ocean at this depth, it may point to fresh, undiscovered hydrothermal venting nearby Station 7 or to heterogeneity in form of the dissolved Fe being transported in the plume away from the EPR.

Finally, the average hydrothermally influenced $\delta^{56}$Fe of +0.54 ± 0.14‰ extended from the 2000 m dFe maximum at both Stations 7 and 4 to the bottom, despite that dFe concentration decreased by as much as 0.5 nmol/kg at depths below 2250 m at Station 7 (33% of maximum dFe) and below 2500 m at Station 4 (57% of maximum dFe). Since the $\delta^{3}$He did not change below the dFe maximum nor downstream at Station 4 (Figure 9), we know with confidence that in the Southeast Pacific, it is scavenging and not dilution that results in the decreasing dFe concentrations above, below, and downstream in the plume. This abyssal dFe scavenging would presumably occur over long time scales (≥residence time of dFe in the ocean) during which time $^{3}$He would continue to mix conservatively, while dFe was scavenged away [*Fitzsimmons et al.*, 2014]. Further evidence for this scavenging mechanism of dFe loss in these deep waters include an absence of vent sources >3000 m depth to explain the deep $^{3}$He data [*Beaulieu et al.*, 2013], implying an advective source for the deep $^{3}$He over long time scales, and the fact that the significantly lower dFe/$^{3}$He ratios that would be required to explain these low dFe concentrations have never been observed [*Fitzsimmons et al.*, 2014; *Resing et al.*, 2015; *Saito et al.*, 2013].

Despite this scavenging of dFe in abyssal waters, no significant change in $\delta^{56}$Fe was observed associated with scavenging removal at either station, suggesting that removal of hydrothermal $\delta^{56}$Fe to the particulate phase is occurring largely without isotope fractionation. However, this observation is inconsistent with the recent findings by *Ellwood et al.* [2015], who inferred that near-crustal ($\delta^{56}$Fe ~ +0.1‰), hydrothermally sourced Fe vented from the Brothers Volcano in the SW Pacific must have been fractionated to isotopically heavy values (greater than +1.5‰) upon scavenging to background abyssal dFe concentrations, with a calculated fractionation factor of −0.67‰. In that study, however, the data did not allow for a distinction between mixing/dilution and scavenging. Thus, the differences between the two studies may be related to this distinction and also to different hydrothermal fluid chemistry, plume biogeochemistry, and background seawater $\delta^{56}$Fe values. Nevertheless, our data do suggest that it may be possible to trace the influence of the EPR in the South Pacific using a relatively conserved, isotopically heavy hydrothermal $\delta^{56}$Fe signature, at least in this region. Future studies will clearly be required to test this further away from the ridge, a focus of already-sailed U.S. and Japanese GEOTRACES section cruises (GP16 and GP19).

As a final note on hydrothermal $\delta^{56}$Fe signatures, we compared the southern EPR plume $\delta^{56}$Fe values of +0.54 ± 0.14‰ measured on BiG RAPA to the +0.02 ± 0.03‰ values measured downstream of the Loihi Seamount hydrothermal system at Station ALOHA on 18 July 2012 (Figure 9). *Fitzsimmons et al.* [2015b] modeled transport of the dFe from Loihi to Station ALOHA, and they observed that a temporally variable transport of hydrothermally derived dFe to Station ALOHA caused a change in the dFe concentration at ~1200 m depth at ALOHA by a factor of 2 (from 0.72 to 1.44 nmol/kg) over 2 years. Unfortunately, no end-member $\delta^{56}$Fe values for Loihi vent fluids have been published that could be used to calculate a fractionation factor during cumulative transformation and transport downstream. Thus, the null hypothesis would be that the ~0‰ $\delta^{56}$Fe measured at Station ALOHA results simply from transport of an ~0‰ Loihi end-member fluid $\delta^{56}$Fe. However, if we assume that the lowest ALOHA dFe of 0.72 nmol/kg measured [*Fitzsimmons et al.*, 2015b] had no hydrothermal contribution (i.e., was just background dFe from remineralization and/or local dFe inputs), then at the time of sampling for Fe isotopes at ALOHA, 42% of the dFe was hydrothermal (0.517 nmol/kg out of 1.235 nmol/kg total dFe) and 58% was non-hydrothermal (0.718 nmol/kg out of 1.235). If we apply the Southeast Pacific $\delta^{56}$Fe values (+0.55‰) to the Loihi component and assume a background AAIW/NPIW $\delta^{56}$Fe of −0.35‰ [*Conway and John*, 2015], then the total dFe of the mixture should have a $\delta^{56}$Fe of +0.02‰, which is identical to the +0.02 ± 0.03‰ value measured.

This calculation suggests that it is plausible that the Loihi distal hydrothermal signature could be similarly heavy to that from the southern EPR.

However, this calculation assumes that the hydrothermal Fe chemistry of the Loihi and southern EPR vents are similar, which is as of yet unclear because of the poor characterization of southern EPR vents currently feeding the BiG RAPA sampling sites. Loihi high-temperature vents are enriched in Fe and $CO_2$ and relatively poor in sulfur [*Glazer and Rouxel*, 2009], with a domination of Fe by Fe(III) compounds and microbial Fe oxidation [*Emerson and Moyer*, 2002]. The low sulfur concentrations have led others to hypothesize that pyrite precipitation occurs prior to venting at Loihi, which would explain the low sulfur and midrange Fe/Mn in Loihi vent fluids [*Wheat et al.*, 2000]; this would cause the Loihi vent fluids to have a potentially heavier $\delta^{56}$Fe upon venting (because the very light $\delta^{56}$Fe of pyrite had been removed), which is in contrast to the more depleted $\delta^{56}$Fe in downstream Loihi plume Fe than southern EPR plume Fe. Southern EPR hydrothermal plumes are variable in chemical composition, but some do contain high Fe and Mn concentrations and very low sulfur, similar to Loihi [*Baker et al.*, 2002]. Thus, further description of what the $\delta^{56}$Fe of downstream dFe can reveal about hydrothermal plume Fe transformations cannot be made until the $\delta^{56}$Fe of vent fluids of the sourcing hydrothermal vents are further characterized.

## 4. Conclusions

In this study we aimed to use dissolved Fe and Fe isotopes to constrain the identity of the Fe fluxes to the Southeast Pacific Ocean, especially extending offshore from the Fe-replete ODZ to the center of the oligotrophic gyre. In the ODZ we observed elevated dFe concentrations to 3.65 nmol/kg that were temporally variable within a factor of 2 over short time scales (~days), with lower dFe concentrations associated with pulses of fresher water. The Fe isotope ($\delta^{56}$Fe) signature of dFe was depleted to $-0.79 \pm 0.03$‰ within the core of the ODZ, consistent with reductive porewater Fe(II) sources to the water column. Surface dFe concentrations were elevated to ~1 nmol/kg, which is elevated but not as high as the ≥50 nmol/kg concentrations recorded along wide continental shelves of the Peruvian ODZ previously, likely because this region had a relatively narrow ODZ that prevented the accumulation of the Fe oxides that might feed such a significant reductively effluxing porewater Fe(II) source. The light $\delta^{56}$Fe of these surface waters (−0.4‰) are consistent with a reductive margin source, as opposed to a dust source that would be isotopically heavy. Isotope excursions in the oxyclines immediately above and below the ODZ to heavier $\delta^{56}$Fe values (+0.45 ± 0.04‰ at 100 m and +0.03 ± 0.04‰ at 500 m) were surprising and must be derived either from sources with heavy $\delta^{56}$Fe signatures (perhaps oxidized margin sediments, which would explain the short-term temporal variability), from the fact that the ODZ directly impinges on anoxic sediments and allows for quantitative Fe release from sediments with a heavy $\delta^{56}$Fe, and/or from FeS precipitation.

Moving offshore into the oligotrophic gyre, dFe concentrations decreased rapidly to <0.1 nmol/kg throughout the upper 400 m of the water column, indicating that the elevated dFe nearshore in the ODZ does not persist very far offshore due to sharp zonal gradients in oxygen concentrations and a lack of a zonal circulation pathway (intermittent eddies being the only case). Offshore surface $\delta^{56}$Fe retained a light, reductive porewater signature >1800 km offshore, but by the middle of the gyre surface $\delta^{56}$Fe was isotopically heavy, perhaps indicative of an influence of dust (isotopically heavy during solubilization) or biological fractionation. However, when published dust fluxes in the region were compared with vertical diffusive Fe fluxes, the vertically diffusing Fe was found to dominate by up to an order of magnitude, proving that recycling of regenerated Fe back upward into the euphotic zone feeds phytoplankton communities more than new dust inputs of Fe. However, both dust and vertical fluxes of Fe to the surface ocean were small compared with the horizontal diffusive fluxes of Fe from the margin, which serve as the dominant source of Fe to the gyre. In the subsurface, while no minimum in dFe was discerned associated with the deep chlorophyll maximum, as in other ocean basins, below the ferricline dFe concentrations were a clear function of remineralization (AOU), with a dFe:C ratio of 4.2 μmol/mol, which is not as low as in Fe-limited ocean regions but not high enough to suggest luxury uptake. This intermediate water layer was found to be relatively fresh AAIW, and the AAIW $\delta^{56}$Fe was observed to be $-0.20 \pm 0.24$‰ (2 SD) across the two stations sampled, illuminating a water mass end-member signature.

In the deep ocean, the elevated dFe concentrations of this study were previously reported to show evidence of distal transport (>2000 km) of hydrothermal Fe from the East Pacific Rise [*Fitzsimmons et al.*, 2014], and so

the $\delta^{56}$Fe data for these samples were used to infer the mechanisms of hydrothermal dFe stabilization. The heavy $\delta^{56}$Fe values of $+0.54 \pm 0.13$‰ in the hydrothermal plume preclude a dominant dFe composition by nanopyrite, which would be expected to be isotopically light (<0‰). Instead, a combination of sulfide precipitation/removal, oxidation of the remaining dFe, and/or binding by organic ligands are believed to have led to the heavy $\delta^{56}$Fe values. Scavenging of dFe was not observed to fractionate Fe isotopes in this study during mixing with abyssal seawater in the distal plume.

In summary, the combined dissolved Fe and Fe isotope data of this study suggest that porewater sources and unique cases of Fe redox cycling over short temporal scales source elevated dFe concentrations to the upwelling region along the Chilean coast. This study provided the first measurements of dissolved Fe below 400 m depth in the South Pacific subtropical gyre, and the Fe isotope data suggest that this Fe derived from reductive margin fluxes nearer to the ODZ and dust inputs in the central ODZ; however, a comparison of measured dust fluxes in this region to the upwelling fluxes through the ferricline suggests that diffusive vertical fluxes of Fe are also critical to maintaining sufficient dFe for surface phytoplankton communities in this gyre. Fe isotopes were also a critical tool for discerning the mechanism of hydrothermal dFe stabilization in the abyssal ocean. The combined approach of dissolved Fe concentrations, physical speciation, and $\delta^{56}$Fe values proved in this study to be a powerful measure of the processes and chemical transformations driving dissolved Fe biogeochemistry in the Southeast Pacific Ocean.

**Acknowledgments**

We thank Filipa Carvalho for the generation of the chlorophyll/station map and Angela Rosenberg for technical assistance at USC. We also thank Dan Repeta (Chief Scientist) and the officers and crew of the R/V *Melville* for a successful sampling program on the BiG RAPA expedition. We thank two anonymous reviewers for aid in improving this manuscript. Data from this project can be found enumerated in the supporting information Table or on BCO-DMO (www.bco-dmo.org). Funding was provided to J.N. Fitzsimmons through an NSF Graduate Research Fellowship (NSF Award 0645960). Research funding was provided by the Center for Microbial Oceanography: Research and Education to E.A. Boyle (NSF-OIA Award EF-0424599) and by the National Science Foundation to S.G. John (OCE 1235150).

## References

Anderson, L. A., and J. L. Sarmiento (1994), Redfield ratios of remineralization determined by nutrient data analysis, *Global Biogeochem. Cycles*, *8*, 65–80, doi:10.1029/93GB03318.

Baker, E. T., et al. (2002), Hydrothermal venting along Earth's fastest spreading center: East Pacific Rise, 27.5–32.3°S, *J. Geophys. Res.*, *107*(B7), 2130, doi:10.1029/2001JB000651.

Beard, B. L., C. M. Johnson, K. L. Von Damm, and R. L. Poulson (2003), Iron isotope constraints on Fe cycling and mass balance in oxygenated Earth oceans, *Geology*, *31*(7), 629–632.

Beaulieu, S. E., E. T. Baker, C. R. German, and A. Maffei (2013), An authoritative global database for active submarine hydrothermal vent fields, *Geochem. Geophys. Geosyst.*, *14*, 4892–4905, doi:10.1002/2013GC004998.

Bell, J., J. Betts, and E. Boyle (2002), MITESS: A moored in situ trace element serial sampler for deep-sea moorings, *Deep Sea Res., Part I*, *49*(11), 2103–2118.

Bennett, S. A., O. Rouxel, K. Schmidt, D. Garbe-Schonberg, P. J. Statham, and C. R. German (2009), Iron isotope fractionation in a buoyant hydrothermal plume, 5°S Mid-Atlantic Ridge, *Geochim. Cosmochim. Acta*, *73*, 5619–5634.

Bergquist, B. A., and E. A. Boyle (2006), Dissolved iron in the tropical and subtropical Atlantic Ocean, *Global Biogeochem. Cycles*, *20*, GB1015, doi:10.1029/2005GB002505.

Blain, S., S. Bonnet, and C. Guieu (2008), Dissolved iron distribution in the tropical and subtropical South Eastern Pacific, *Biogeosciences*, *5*(1), 269–280.

Bonnet, S., et al. (2008), Nutrient limitation of primary productivity in the Southeast Pacific (BIOSOPE cruise), *Biogeosciences*, *5*, 215–225.

Broecker, W. S. (1974), *Chemical Oceanography*, Harcourt Publishers, New York.

Broecker, W. S., S. Blanton, W. M. Smethie, and H. G. Ostlund (1991), Radiocarbon decay and oxygen utilization in the deep Atlantic Ocean, *Global Biogeochem. Cycles*, *5*, 87–117, doi:10.1029/90GB02279.

Bruland, K. W., E. L. Rue, and G. J. Smith (2001), Iron and macronutrients in California coastal upwelling regimes: Implications for diatom blooms, *Limnol. Oceanogr.*, *46*(7), 1661–1674.

Bruland, K. W., E. L. Rue, G. J. Smith, and G. R. DiTullio (2005), Iron, macronutrients and diatom blooms in the Peru upwelling regime: Brown and blue waters of Peru, *Mar. Chem.*, *93*, 81–103.

Buck, C. S., W. M. Landing, and J. Resing (2013), Pacific Ocean aerosols: Deposition and solubility of iron, aluminum, and other trace elements, *Mar. Chem.*, *157*, 117–130.

Bullen, T. D., A. F. White, C. W. Childs, D. V. Vivit, and M. S. Schulz (2001), Demonstration of significant abiotic iron isotope fractionation in nature, *Geology*, *29*(8), 699–702.

Bundy, R. M., K. A. Barbeau, D. V. Biller, K. N. Buck, and K. W. Bruland (2014), Distinct pools of dissolved iron-binding ligands in the surface and benthic boundary layer of the California Current, *Limnol. Oceanogr.*, *59*, 769–787.

Carr, M.-E. (2001), Estimation of potential productivity in Eastern Boundary Currents using remote sensing, *Deep Sea Res. Part II: Top. Studies Oceanogr.*, *49*(1–3), 59–80.

Chever, F., O. J. Rouxel, P. L. Croot, E. Ponzevera, K. Wuttig, and M. Auro (2015), Total dissolvable and dissolved iron isotopes in the water column of the Peru upwelling regime, *Geochim. Cosmochim. Acta*, *162*, 66–82.

Claustre, H., A. Sciandra, and D. Vaulot (2008), Introduction to the special section bio-optical and biogeochemical conditions in the South East Pacific in late 2004: The BIOSOPE program, *Biogeosciences*, *5*, 679–691.

Conway, T. M., and S. G. John (2014), Quantification of dissolved iron sources to the North Atlantic Ocean, *Nature*, *511*, 212–215.

Conway, T. M., and S. G. John (2015), The cycling of iron, zinc and cadmium in the North East Pacific Ocean—Insights from stable isotopes, *Geochim. Cosmochim. Acta*, *164*, 262–283.

Conway, T. M., A. D. Rosenberg, J. F. Adkins, and S. G. John (2013), A new method for precise determination of iron, zinc, and cadmium stable isotope ratios in seawater by double-spike mass spectrometry, *Anal. Chim. Acta*, *793*, 44–52.

Conway, T. M., S. G. John, and F. Lacan (2016), Intercomparison of dissolved iron isotope profiles from re-occupation of three GEOTRACES stations in the Atlantic Ocean, *Mar. Chem.*, *183*, 50–61.

Czeschel, R., L. Stramma, F. U. Schwarzkopf, B. S. Giese, A. Funk, and J. Karstensen (2011), Middepth circulation of the eastern tropical South Pacific and its link to the oxygen minimum zone, *J. Geophys. Res.*, *116*, C01015, doi:10.1029/2010JC006565.

Draxler, R. R., and G. D. Rolph (2014), HYSPLIT (HYbrid Single-Particle Lagrangian Integrated Trajectory) Model access via NOAA ARL READY Website [Available at http://ready.arl.noaa.gov/HYSPLIT.php], NOAA Air Resources Laboratory, Silver Spring, Md.
Ellwood, M. J., S. D. Nodder, A. L. King, D. A. Hutchins, S. W. Wilhelm, and P. W. Boyd (2014), Pelagic iron cycling during the subtropical spring bloom, east of New Zealand, *Mar. Chem.*, *160*, 18–33.
Ellwood, M. J., D. A. Hutchins, M. C. Lohan, A. Milne, P. Nasemann, S. D. Nodder, S. G. Sander, R. Strzepek, S. W. Wilhelm, and P. W. Boyd (2015), Iron stable isotopes track pelagic iron cycling during a subtropical phytoplankton bloom, *Proc. Natl. Acad. Sci. U.S.A.*, *112*(1), E15–E20.
Emerson, D., and C. L. Moyer (2002), Neutrophilic Fe-oxidizing bacteria are abundant at the Loihi Seamount hydrothermal vents and play a major role in Fe oxide deposition, *Appl. Environ. Microbiol.*, *68*(6), 3085–3093.
Fiedler, P. C., and L. D. Talley (2006), Hydrography of the eastern tropical Pacific: A review, *Prog. Oceanogr.*, *69*, 143–180.
Field, M. P., and R. M. Sherrell (2000), Dissolved and particulate Fe in a hydrothermal plume at 9°45′N, East Pacific Rise: Slow Fe (II) oxidation kinetics in Pacific plumes, *Geochim. Cosmochim. Acta*, *64*(4), 619–628.
Fitzsimmons, J. N., and E. A. Boyle (2012), An intercalibration between the GEOTRACES GO-FLO and the MITESS/Vanes sampling systems for dissolved iron concentration analyses (and a closer look at adsorption effects), *Limnol. Oceanogr. Methods*, *10*, 437–450.
Fitzsimmons, J. N., and E. A. Boyle (2014), Both soluble and colloidal iron phases control dissolved iron variability in the tropical North Atlantic Ocean, *Geochim. Cosmochim. Acta*, *125*, 539–550.
Fitzsimmons, J. N., R. Zhang, and E. A. Boyle (2013), Dissolved iron in the tropical North Atlantic oxygen minimum zone, *Mar. Chem.*, *154*, 87–99.
Fitzsimmons, J. N., W. J. Jenkins, and E. A. Boyle (2014), Distal transport of dissolved hydrothermal iron in the deep South Pacific Ocean, *Proc. Natl. Acad. Sci. U.S.A.*, *111*(47), 16,654–16,661.
Fitzsimmons, J. N., R. M. Bundy, S. N. Al-Subiai, K. A. Barbeau, and E. A. Boyle (2015a), The composition of dissolved iron in the dusty surface ocean: An exploration using size-fractionated iron-binding ligands, *Mar. Chem.*, *173*, 125–135.
Fitzsimmons, J. N., C. T. Hayes, S. N. Al-Subiai, R. Zhang, P. L. Morton, R. E. Weisend, F. Ascani, and E. A. Boyle (2015b), Daily to decadal variability of size-fractionated iron and iron-binding ligands at the Hawaii Ocean Time-series Station ALOHA, *Geochim. Cosmochim. Acta*, *171*, 303–324.
Fitzsimmons, J. N., G. G. Carrasco, J. Wu, S. Roshan, M. Hatta, C. I. Measures, T. M. Conway, S. G. John, and E. A. Boyle (2015c), Partitioning of dissolved iron and iron isotopes into soluble and colloidal phases along the GA03 GEOTRACES North Atlantic Transect, *Deep Sea Res., Part II*, *116*, 130–151.
Fuenzalida, R., W. Schneider, J. Garces-Vargas, L. Bravo, and C. Lange (2009), Vertical and horizontal extension of the oxygen minimum zone in the eastern South Pacific Ocean, *Deep Sea Res., Part II*, *56*, 992–1003.
Gargett, A. E. (1984), Vertical eddy diffusivity in the ocean interior, *J. Mar. Res.*, *42*, 359–393.
Gartman, A., A. J. Findlay, and G. W. Luther III (2014), Nanoparticulate pyrite and other nanoparticles are a widespread component of hydrothermal vent black smoker emissions, *Chem. Geol.*, *366*, 32–41.
Glazer, B. T., and O. J. Rouxel (2009), Redox speciation and distribution within diverse iron-dominated microbial habitats at Loihi Seamount, *Geomicrobiol. J.*, *26*, 606–622.
Hatta, M., C. I. Measures, S. Roshan, J. Wu, J. N. Fitzsimmons, P. Sedwick, and P. L. Morton (2015), An overview of dissolved Fe and Mn distributions during the 2010–2011 U.S. GEOTRACES North Atlantic cruises: GEOTRACES GA03, *Deep Sea Res., Part II*, *116*, 117–129.
Hawkes, J. A., D. P. Connelly, M. Gledhill, and E. P. Achterberg (2013), The stabilisation and transportation of dissolved iron from high temperature hydrothermal vent systems, *Earth Planet. Sci. Lett.*, *375*, 280–290.
Helly, J. J., and L. A. Levin (2004), Global distribution of naturally occurring marine hypoxia on continental margins, *Deep Sea Res., Part I*, *51*, 1159–1168.
Homoky, W. B., S. Severmann, R. A. Mills, P. J. Statham, and G. R. Fones (2009), Pore-fluid Fe isotopes reflect the extent of benthic Fe redox recycling: Evidence from continental shelf and deep-sea sediments, *Geology*, *37*(8), 751–754.
Homoky, W. B., S. G. John, T. M. Conway, and R. A. Mills (2013), Distinct iron isotopic signatures and supply from marine sediment dissolution, *Nat. Commun.*, *4*, 2143, doi:10.1038/ncomms3143.
Hong, H., and D. R. Kester (1986), Redox state of iron in the offshore waters of Peru, *Limnol. Oceanogr.*, *31*(3), 512–524.
Jenkins, W. J., W. M. Smethie, E. A. Boyle, and G. A. Cutter (2015), Water mass analysis for the U.S. GEOTRACES (GA03) North Atlantic sections, *Deep Sea Res., Part II*, *116*, 6–20.
John, S. G. (2012), Optimizing sample and spike concentrations for isotopic analysis by double-spike ICPMS, *J. Anal. At. Spectrom.*, *27*(12), 2123–2131.
John, S. G., and J. Adkins (2012), The vertical distribution of iron stable isotopes in the North Atlantic near Bermuda, *Global Biogeochem. Cycles*, *26*, GB2034, doi:10.1029/2011GB004043.
John, S. G., J. Mendez, J. Moffett, and J. Adkins (2012), The flux of iron and iron isotopes from San Pedro Basin sediments, *Geochim. Cosmochim. Acta*, *93*, 14–29.
Johnson, C. M., J. L. Skulan, B. L. Beard, H. Sun, K. H. Nealson, and P. S. Braterman (2002), Isotopic fractionation between Fe(III) and Fe(II) in aqueous solutions, *Earth Planet. Sci. Lett.*, *195*(1–2), 141–153.
Karstensen, J., L. Stramma, and M. Visbeck (2008), Oxygen minimum zones in the eastern tropical Atlantic and Pacific oceans, *Prog. Oceanogr.*, *77*, 331–350.
Labatut, M., F. Lacan, C. Pradoux, J. Chmeleff, A. Radic, J. W. Murray, F. Poitrasson, A. M. Johansen, and F. Thil (2014), Iron sources and dissolved-particulate interactions in the seawater of the Western Equatorial Pacific, iron isotope perspectives, *Global Biogeochem. Cycles*, *28*, 1044–1065, doi:10.1002/2014GB004928.
Lacan, F., A. Radic, C. Jeandel, F. Poitrasson, G. Sarthou, C. Pradoux, and R. Freydier (2008), Measurement of the isotopic composition of dissolved iron in the open ocean, *Geophys. Res. Lett.*, *35*, L24610, doi:10.1029/2008GL035841.
Ledwell, J. R., A. J. Watson, and C. S. Law (1998), Mixing of a tracer in the pycnocline, *J. Geophys. Res.*, *103*, 21,499–21,529, doi:10.1029/98JC01738.
Lee, J.-M., E. A. Boyle, Y. Echegoyen-Sanz, J. N. Fitzsimmons, R. Zhang, and R. A. Kayser (2011), Analysis of trace metals (Cu, Cd, Pb, and Fe) in seawater using single batch Nitrilotriacetate resin extraction and isotope dilution inductively coupled plasma mass spectrometry, *Anal. Chim. Acta*, *686*, 93–101.
Llanillo, P. J., J. Karstensen, J. L. Pelegrí, and L. Stramma (2013), Physical and biogeochemical forcing of oxygen and nitrate changes during El Niño/El Viejo and La Niña/La Vieja upper-ocean phases in the tropical eastern South Pacific along 86° W, *Biogeosciences*, *10*, 6339–6355.
Loscher, B. M., H. J. W. De Baar, J. T. M. De Jong, C. Veth, and F. Dehairs (1997), The distribution of Fe in the antarctic circumpolar current, *Deep Sea Res., Part II*, *44*(1–2), 143–187.
Mackas, D. K., K. L. Denman, and A. F. Bennett (1987), Least squares multiple tracer analysis of water mass composition, *J. Geophys. Res.*, *92*, 2907–2918, doi:10.1029/JC092iC03p02907.

Martin, J. H., and S. E. Fitzwater (1988), Iron deficiency limits phytoplankton growth in the north-east Pacific subarctic, *Nature*, *331*, 341–343.
Martin, J. H., G. A. Knauer, D. M. Karl, and W. W. Broenkow (1987), VERTEX: Carbon cycling in the northeast Pacific, *Deep Sea Res., Part A*, *34*(2), 267–285.
Martin, J. H., R. M. Goron, S. Fitzwater, and W. W. Broenkow (1989), VERTEX: Phytoplankton/iron studies in the Gulf of Alaska, *Deep Sea Res., Part A*, *36*(5), 649–680.
Martin, J. H., S. E. Fitzwater, R. Michael Gordon, C. N. Hunter, and S. J. Tanner (1993), Iron, primary production and carbon-nitrogen flux studies during the JGOFS North Atlantic bloom experiment, *Deep Sea Res., Part II*, *40*(1–2), 115–134.
Mawji, E., et al. (2015), The GEOTRACES Intermediate Data Product 2014, *Mar. Chem.*, *177*(Part 1), 1–8.
Mead, C., P. Herckes, B. J. Majestic, and A. D. Anbar (2013), Source apportionment of aerosol iron in the marine environment using iron isotope analysis, *Geophys. Res. Lett.*, *40*, 5722–5727, doi:10.1002/2013GL057713.
Moffett, J. W., T. J. Goepfert, and S. W. A. Naqvi (2007), Reduced iron associated with secondary nitrite maxima in the Arabian Sea, *Deep Sea Res., Part I*, *54*(8), 1341–1349.
Moore, J. K., and O. Braucher (2008), Sedimentary and mineral dust sources of dissolved iron to the world ocean, *Biogeosciences*, *5*, 631–656.
Moore, J. K., S. C. Doney, D. M. Glover, and I. Y. Fung (2002), Iron cycling and nutrient-limitation patterns in surface waters of the World Ocean, *Deep Sea Res., Part II*, *49*(1-3), 463–507.
Morel, F. M. M., A. B. Kustka, and Y. Shaked (2008), The role of unchelated Fe in the iron nutrition of phytoplankton, *Limnol. Oceanogr.*, *53*(1), 400–404.
Morgan, J. L. L., L. E. Wasylenki, J. Nuester, and A. D. Anbar (2010), Fe isotope fractionation during equilibration of Fe-organic complexes, *Environ. Sci. Technol.*, *44*(16), 6095–6101.
Noble, A. E., et al. (2012), Basin-scale inputs of cobalt, iron, and manganese from the Benguela-Angola front to the South Atlantic Ocean, *Limnol. Oceanogr.*, *57*(4), 989–1010.
Okubo, A. (1971), Oceanic diffusion diagrams, *Deep Sea Res. Oceanogr. Abstr.*, *18*, 789–802.
Poitrasson, F. (2006), On the iron isotope homogeneity level of the continental crust, *Chem. Geol.*, *235*(1–2), 195–200.
Radic, A., F. Lacan, and J. W. Murray (2011), Iron isotopes in the seawater of the equatorial Pacific Ocean: New constraints for the oceanic iron cycle, *Earth Planet. Sci. Lett.*, *306*, 1–10.
Reid, J. L. (1997), On the total geostrophic circulation of the south Pacific Ocean: Flow patterns, tracers and transports, *Prog. Oceanogr.*, *39*, 263–352.
Resing, J. A., P. N. Sedwick, C. R. German, W. J. Jenkins, J. W. Moffett, B. M. Sohst, and A. Tagliabue (2015), Basin-scale transport of hydrothermal dissolved metals across the South Pacific Ocean, *Nature*, *523*, 200–206.
Rijkenberg, M. J. A., S. Steigenberger, C. F. Powell, H. V. Haren, M. D. Patey, A. R. Baker, and E. P. Achterberg (2012), Fluxes and distribution of dissolved iron in the eastern (sub-) tropical North Atlantic, *Global Biogeochem. Cycles*, *26*, GB3004, doi:10.1029/2011GB004264.
Rouxel, O., E. Sholkovitz, M. Charette, and K. J. Edwards (2008a), Iron isotope fractionation in subterranean estuaries, *Geochim. Cosmochim. Acta*, *72*(14), 3413–3430.
Rouxel, O., W. C. Shanks Iii, W. Bach, and K. J. Edwards (2008b), Integrated Fe- and S-isotope study of seafloor hydrothermal vents at East Pacific Rise 9–10°N, *Chem. Geol.*, *252*(3–4), 214–227.
Rouxel, O., B. M. Toner, S. J. Manganini, and C. R. German (2016), Geochemistry and iron isotope systematics of hydrothermal plume fall-out at East Pacific Rise 9°50′N, *Chem. Geol.*, *441*, 212–234.
Roy, M., O. Rouxel, J. B. Martin, and J. E. Cable (2012), Iron isotope fractionation in a sulfide-bearing subterranean estuary and its potential influence on oceanic Fe isotope flux, *Chem. Geol.*, *300–301*, 133–142.
Saito, M. A., A. E. Noble, A. Tagliabue, T. J. Goepfert, C. H. Lamborg, and W. J. Jenkins (2013), Slow-spreading submarine ridges in the South Atlantic as a significant oceanic iron source, *Nat. Geosci.*, *6*, 775–779.
Sander, S. G., and A. Koschinsky (2011), Metal flux from hydrothermal vents increased by organic complexation, *Nat. Geosci.*, *4*, 145–150.
Schlosser, C., P. Streu, and P. L. Croot (2013), Vivaspin ultrafiltration: A new approach for high resolution measurements of colloidal and soluble iron species, *Limnol. Oceanogr. Methods*, *11*, 187–201.
Scholz, F., C. Hensen, A. Noffke, A. Rohde, V. Liebetrau, and K. Wallmann (2011), Early diagenesis of redox-sensitive trace metals in the Peru upwelling area—Response to ENSO-related oxygen fluctuations in the water column, *Geochim. Cosmochim. Acta*, *75*, 7257–7276.
Scholz, F., S. Severmann, J. McManus, and C. Hensen (2014), Beyond the Black Sea paradigm: The sedimentary fingerprint of an open-marine iron shuttle, *Geochim. Cosmochim. Acta*, *127*, 368–380.
Sedwick, P. N., T. M. Church, A. R. Bowie, C. M. Marsay, S. J. Ussher, K. M. Achilles, P. J. Lethaby, R. J. Johnson, M. M. Sarin, and D. J. McGillicuddy (2005), Iron in the Sargasso Sea (Bermuda Atlantic Time-series Study region) during summer: Eolian imprint, spatiotemporal variability, and ecological implications, *Global Biogeochem. Cycles*, *19*, GB4006, doi:10.1029/2004GB002445.
Sedwick, P. N., E. R. Sholkovitz, and T. M. Church (2007), Impact of anthropogenic combustion emissions on the fractional solubility of aerosol iron: Evidence from the Sargasso Sea, *Geochem. Geophys. Geosyst.*, *8*, Q10Q06, doi:10.1029/2007GC001586.
Sedwick, P. N., B. M. Sohst, S. J. Ussher, and A. R. Bowie (2015), A zonal picture of the water column distribution of dissolved iron(II) during the U.S. GEOTRACES North Atlantic transect cruise (GEOTRACES GA03), *Deep Sea Res., Part II*, *116*, 166–175.
Severmann, S., C. M. Johnson, B. L. Beard, C. R. German, H. N. Edmonds, H. Chiba, and D. R. H. Green (2004), The effect of plume processes on the Fe isotope composition of hydrothermally derived Fe in the deep ocean as inferred from the Rainbow vent site, Mid-Atlantic Ridge, 36 degrees 14′ N, *Earth Planet. Sci. Lett.*, *225*(1–2), 63–76.
Severmann, S., C. M. Johnson, B. L. Beard, and J. McManus (2006), The effect of early diagenesis on the Fe isotope compositions of porewaters and authigenic minerals in continental margin sediments, *Geochim. Cosmochim. Acta*, *70*, 2006–2022.
Severmann, S., J. McManus, W. M. Berelson, and D. E. Hammond (2010), The continental shelf benthic iron flux and its isotope composition, *Geochim. Cosmochim. Acta*, *74*, 3984–4004.
Siebert, C., T. F. Nägler, and J. D. Kramers (2001), Determination of molybdenum isotope fractionation by double-spike multicollector inductively coupled plasma mass spectrometry, *Geochem. Geophys. Geosyst.*, *2*, 1032, doi:10.1029/2000GC000124.
Silva, N., N. Rojas, and A. Fedele (2009), Water masses in the Humboldt Current System: Properties, distribution, and the nitrate deficit as a chemical water mass tracer for Equatorial Subsurface Water off Chile, *Deep Sea Res., Part II*, *56*, 1004–1020.
Sivan, O., M. Adler, A. Pearson, F. Gelman, I. Bar-Or, S. G. John, and W. Eckert (2011), Geochemical evidence for iron-mediated anaerobic oxidation of methane, *Limnol. Oceanogr.*, *56*(4), 1536–1544.
Skulan, J. L., B. L. Beard, and C. M. Johnson (2002), Kinetic and equilibrium Fe isotope fractionation between aqueous Fe(III) and hematite, *Geochim. Cosmochim. Acta*, *66*, 2995–3015.
Staubwasser, M., R. Schoenberg, F. von Blanckenburg, S. Krüger, and C. Pohl (2013), Isotope fractionation between dissolved and suspended particulate Fe in the oxic and anoxic water column of the Baltic Sea, *Biogeosciences*, *10*(1), 233–245.

Steele, R. C. J., T. Elliott, C. D. Coath, and M. Regelous (2011), Confirmation of mass-independent Ni isotopic variability in iron meteorites, *Geochim. Cosmochim. Acta*, *75*(24), 7906–7925.
Sunda, W. G. (1997), Control of dissolved iron concentrations in the world ocean: A comment, *Mar. Chem.*, *57*(3–4), 169–172.
Sunda, W. G. (2012), Feedback interactions between trace metal nutrients and phytoplankton in the ocean, *Front. Microbiol.*, *3*, 204.
Tagliabue, A., et al. (2010), Hydrothermal contribution to the oceanic dissolved iron inventory, *Nat. Geosci.*, *3*(4), 252–256.
Tagliabue, A., T. Mtshali, O. Aumont, A. R. Bowie, M. B. Klunder, A. N. Roychoudhury, and S. Swart (2012), A global compilation of dissolved iron measurements: Focus on distributions and processes in the Southern Ocean, *Biogeosciences*, *9*, 2333–2349.
Talley, L. D., G. L. Pickard, W. J. Emery, and J. H. Swift (2011), *Descriptive Physical Oceanography*, 6th ed., Elsevier, San Diego, Calif.
Tomczak, M. (1981), A multi-parameter extension of temperature/salinity diagram techniques for the analysis of non-isopycnal mixing, *Prog. Oceanogr.*, *10*, 147–171.
Toner, B. M., M. A. Marcus, K. J. Edwards, O. Rouxel, and C. R. German (2012), Measuring the form of iron in hydrothermal plume particles, *Oceanography*, *25*(1), 209–212.
Ulloa, O., D. E. Canfield, E. F. DeLong, R. F. Letelier, and F. J. Steward (2012), Microbial oceanogrpahy of anoxic oxygen minimum zones, *Proc. Natl. Acad. Sci. U.S.A.*, *109*, 15,996–16,003.
Vedamati, J., T. Goepfert, and J. W. Moffett (2014), Iron speciation in the eastern tropical South Pacific oxygen minimum zone off Peru, *Limnol. Oceanogr.*, *59*(6), 1945–1957.
Waeles, M., A. R. Baker, T. Jickells, and J. Hoogewerff (2007), Global dust teleconnections: aerosol iron solubility and stable isotope composition, *Environ. Chem.*, *4*(4), 233–237.
Wagener, T., C. Guieu, R. Losno, S. Bonnet, and N. Mahowald (2008), Revisiting atmospheric dust export to the Southern Hemisphere ocean: Biogeochemical implications, *Global Biogeochem. Cycles*, *22*, GB2006, doi:10.1029/2007GB002984.
Welch, S. A., B. L. Beard, C. M. Johnson, and P. S. Braterman (2003), Kinetic and equilibrium Fe isotopic fractionation between aqueous Fe(II) and Fe(III), *Geochim. Cosmochim. Acta*, *67*(22), 4231–4250.
Wheat, C. G., H. W. Jannasch, J. N. Plant, C. L. Moyer, F. J. Sansone, and G. M. McMurtry (2000), Continuous sampling of hydrothermal fluids from Loihi Seamount after the 1996 event, *J. Geophys. Res.*, *105*, 19,353–19,367, doi:10.1029/2000JB900088.
Yucel, M., A. Gartman, C. S. Chan, and G. W. Luther (2011), Hydrothermal vents as a kinetically stable source of iron-sulphide-bearing nanoparticles to the ocean, *Nat. Geosci.*, *4*, 367–371.